INORGANIC CHEMISTRY

FRONTIERS

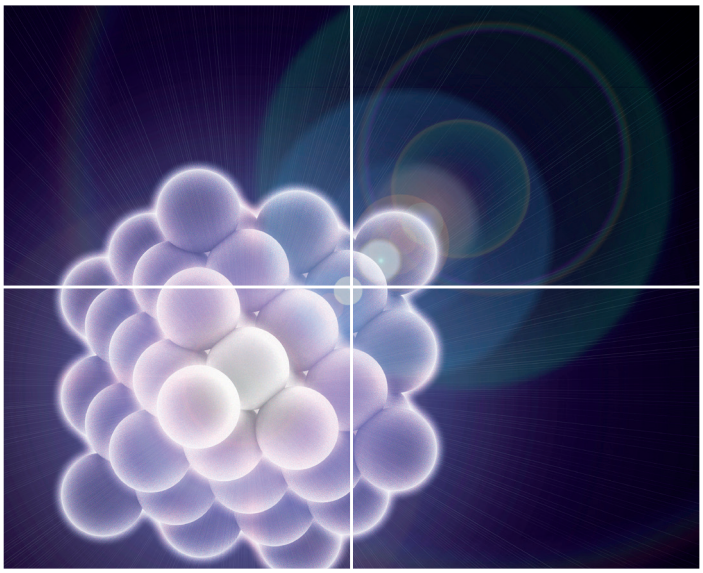

Accepted Manuscript

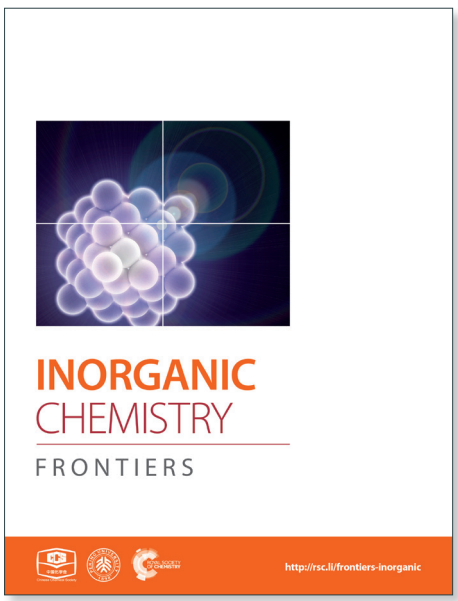

This is an *Accepted Manuscript*, which has been through the Royal Society of Chemistry peer review process and has been accepted for publication.

Accepted Manuscripts are published online shortly after acceptance, before technical editing, formatting and proof reading. Using this free service, authors can make their results available to the community, in citable form, before we publish the edited article. We will replace this *Accepted Manuscript* with the edited and formatted *Advance Article* as soon as it is available.

You can find more information about *Accepted Manuscripts* in the **Information for Authors**.

Please note that technical editing may introduce minor changes to the text and/or graphics, which may alter content. The journal's standard **Terms & Conditions** and the **Ethical guidelines** still apply. In no event shall the Royal Society of Chemistry be held responsible for any errors or omissions in this *Accepted Manuscript* or any consequences arising from the use of any information it contains.

DNA/protein binding, DNA cleavage, cytotoxicity, superoxide radical scavenging and molecular docking studies of copper(II) complexes containing *N*-benzyl-*N′*-aryl-*N″*-benzoylguanidine ligands

Kumaramangalam Jeyalakshmi,[a] Yuvaraj Arun,[b] Nattamai S. P. Bhuvanesh,[c] Paramasivan Thirumalai Perumal,[b] Anantharaman Sreekanth[a] and Ramasamy Karvembu[a*]

Abstract

Five copper(II) complexes containing *N*,*N'*,*N''*-trisubstituted guanidine ligands were synthesized and characterized by elemental analyses, and UV-Visible, FT-IR, EPR and mass spectroscopic techniques. The synthesized copper(II) complexes (**1**-**5**) bear the general formula $[Cu\{C_6H_5CONC(NR)NHCH_2C_6H_5\}_2]$ where R = phenyl (**1**), 4-methylphenyl (**2**), 4-ethoxyphenyl (**3**), 2-methoxyphenyl (**4**) or 1-naphthyl (**5**). Four coordinated square planar geometry of the complexes was confirmed by single crystal X-ray diffraction study. The interaction of the Cu(II) complexes with calf thymus DNA (CT DNA) was explored using absorption and fluorescence spectroscopic methods. The results revealed that the complexes have an affinity constant for DNA in the order of 10^4 M^{-1} and the mode of interaction is non covalent intercalation. DNA cleavage study showed that the complexes cleaved DNA without any external agent. The interaction of Cu(II) complexes with bovine serum albumin (BSA) was also studied using absorption and fluorescence techniques. The cytotoxic activity of the Cu(II) complexes was probed *in vitro* against human breast (MCF7) and lung (A549) cancer cell lines. The complexes were also tested against mouse embryonic fibroblasts (NIH 3T3) cell lines. The complexes **1** and **3** have good cytotoxic activity which is comparable with cyclophosphamide drug. The complexes were less cytotoxic towards normal cell lines showing that they affect only cancer cell lines. Superoxide radical scavenging properties of the complexes were assessed using NBT assay. Copper(II) complexes showed appreciable superoxide radical scavenging activity with IC_{50} value ranging from 1.53 to 5.62 μM. Further molecular docking technique was employed to understand the binding of the complexes toward the molecular target DNA and human DNA topoisomerase I.

---

[a] *Department of Chemistry, National Institute of Technology, Tiruchirappalli - 620015, India. E-mail address: kar@nitt.edu (R. Karvembu); Fax: +91 431 2500133; Tel: +91 431 2503631*

[b] *Organic Chemistry Division, CSIR-Central Leather Research Institute, Chennai - 600020, India*

[c] *Department of Chemistry, Texas A & M University, College Station, TX 77842, USA*

Electronic supplementary information (ESI) available: Electronic absorption spectra of complexes **2**, **4** and **5** upon addition of DNA (Fig. S1), emission spectra of DNA-EB in the presence of complexes **2**, **4** and **5** (Fig. S2), fluorescence quenching curves of BSA with complexes **1**, **2** and **4** (Fig. S3), synchronous spectra ($\Delta\lambda$ = 15 and 60 nm) of complexes **1**, **2** and **4** with BSA (Figs. S4 and S5) and cytotoxicity of the complexes against normal cells (Fig. S6). Crystallographic data for the structures reported in this paper have been deposited with the Cambridge Crystallographic Data Centre (CCDC) as supplementary publication numbers CCDC 1023785-1023791. Copies of the data can be obtained free of charge from the CCDC (12 Union Road, Cambridge CB2 1EZ, UK; Tel.: + 44-1223-336408; Fax: + 44-1223-336003; e-mail: deposit@ccdc.cam.ac.uk; web site: http://www.ccdc.cam.ac.uk).

1. Introduction

Synthesis of new transition metal complexes possessing the analogous properties of anticancer drug is a fascinating area of research in bioinorganic chemistry. The electron-rich nature of biomolecules (DNA/protein) and electron-deficient metal ions are believed to have strong interactions, which are thought to be the criteria for the pharmaceutical activities of the complexes. Therefore, the study of the binding properties of metal complexes with DNA and protein is of great significance for the design of new drugs and their application.[1]

DNA is one of the main molecular targets in the design of anticancer compounds.[2] DNA-binding small molecules have attracted interest because of their interference with important mechanisms in the cell, some inducing mutations and cancer, while others have found use as cancer therapeutics. Further, it has been revealed that free radicals can damage proteins, lipids and DNA of bio-tissues, leading to increased rates of cancer and fortunately antioxidants can prevent this damage due to their free radical scavenging activity.[3,4] Therefore much attention has been given to metal complexes that can bind to DNA and also with antioxidant properties.

At the same time, proteins have also attracted enormous research interest as a prime molecular target.[5] Serum albumins such as bovine serum albumin (BSA) is the most important protein present in plasma that carries several endo- and exogenous compounds.[5] It is essential to explore drug-protein interactions as most of the drugs bound to serum albumin are usually transported as a protein complex.[6,7] Attention has also been focused on the

proteins that drive and control cell cycle progression.[8] Therefore interaction studies of the metal complexes with proteins like BSA become very important to develop drugs with great potential.

The guanidine molecule, $(NH_2)_2C=NH$, is an important ingredient of both organic and inorganic chemistry. Guanidine is noted as sterically and electronically flexible ligand because of the Y-shaped CN_3 unit present in it. The guanidine group is a decisive feature in many biologically active species such as arginine, triazabicyclodecene and saxitoxin. It is found in a growing number of biologically and pharmaceutically relevant compounds. Due to its large spectrum of biological activity the guanidine functional group has been intensively studied as a synthetic goal. Guanidines have broad spectrum of biological activities like antitumour[9-11], antimalarial, antiinflammatory, urease inhibition[12], etc. This is further enhanced by coordination with metal. A large number of guanidine complexes has been reported with different metals like Cu, Pt, Co, Ni, Ru, Fe, Zn and so on.[13,14] But copper has special importance compared to other metals. Copper is an essential element for most aerobic organisms, employed as a structural and catalytic cofactor, and consequently it is involved in many biological pathways.[15-17] Also, serum copper levels correlate with tumor incidence, tumor weight, malignant progression, and recurrence in a variety of human cancers supporting the idea that copper could be used as a potential tumor-specific target. Several copper complexes[18-31] have been now proposed as potential anticancer substances and cancer inhibiting agents, as they showed remarkable anticancer activity and lower general toxicity than platinum compounds. All the above facts have motivated us to develop copper complexes containing *N*,*N*′,*N*″-trisubstituted guanidine ligands and to evaluate their DNA binding, DNA cleavage, protein binding, cytotoxicity and superoxide radical scavenging properties.

2. Results and discussion

2.1 Synthesis and characterization

The substituted thiourea was synthesized from benzoyl chloride and benzylamine using the standard procedure.[32] The trisubstituted guanidine ligands were obtained from the mercury promoted guanylation reaction between *N*-benzoyl-*N*′-benzylthiourea and the suitable amine (Scheme 1).[33,34] The synthesis of copper(II) complexes were achieved in good yields by the reaction of guanidine ligands with copper acetate monohydrate. (Scheme 2)

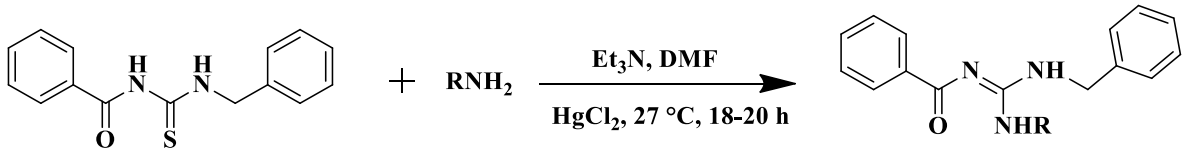

R=C_6H_5 (L1), *p*-$C_6H_4CH_3$ (L2), *p*-$C_6H_4OC_2H_5$ (L3), *o*-$C_6H_4OCH_3$ (L4) or $C_{10}H_7$ (L5)

Scheme 1. Synthesis of *N*-benzyl-*N′*-aryl-*N″*-benzoylguanidine

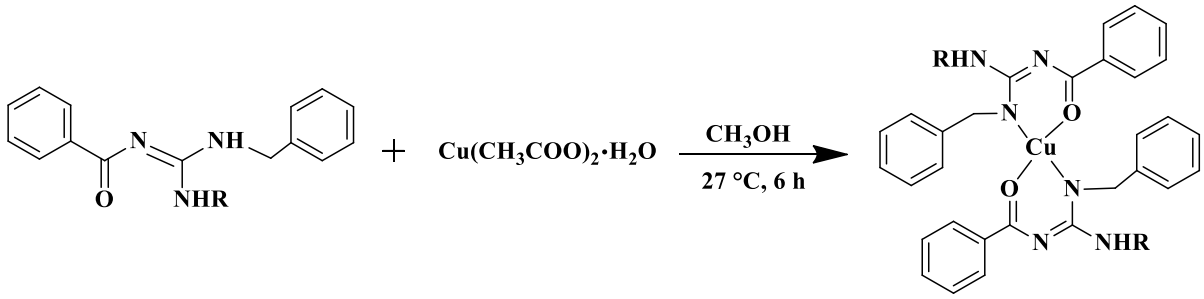

R=C_6H_5 (1), *p*-$C_6H_4CH_3$ (2), *p*-$C_6H_4OC_2H_5$ (3), *o*-$C_6H_4OCH_3$ (4) or $C_{10}H_7$ (5)

Scheme 2. Synthesis of copper(II) complexes

The synthesized ligands and complexes were characterized using UV-Visible, FT-IR, NMR/EPR and mass/elemental analyses techniques. The electronic spectra of the ligands showed bands around 272-290 and 235-268 nm regions, which correspond to $\pi\rightarrow\pi^*$ and $n\rightarrow\pi^*$ transitions respectively. In the complexes, a band appeared around 240-271 nm corresponds to intraligand transition. Ligand to metal charge transfer transition (LMCT) is characterized by the appearance of a band around 377-389 nm. There is a broad band around 592-643 nm which is characteristic of d→d transition.[35]

In the FT-IR spectra of the ligands there are two N−H bands appeared around 3165-3419 cm^{-1}. One of the N−H bands is sharp and another one is weak. The weak N−H band is due to the involvement of hydrogen bonding between the carbonyl oxygen and the N−H hydrogen. The C=N absorbs around 1561-1571 cm^{-1} and C=O absorbs around 1591-1602 cm^{-1}.[36] On complexation there is a shift in the C=O stretching frequency towards the lower value and there is a disappearance of the weak N−H band. This clearly confirms that the coordination occurs through carbonyl oxygen and the nitrogen of the N−H after deprotonation.

In the ^{1}H NMR spectra of the ligands (L1-L5), the signal of the N−HR proton appears in the downfield around 12.54-11.93 ppm since it is attached to an aromatic ring. The N−H proton attached to the benzyl moiety appears in the upfield around 5.22-5.10 ppm. The benzyl CH_2 proton resonates around 4.74-4.81 ppm. The signals due to all the other aromatic protons are in the expected range. ^{13}C NMR spectra of the ligands confirm the presence of C=O (178.1-177.7 ppm) and C=N (159.6-158.1 ppm) carbons. Chemical shifts of all the other aromatic and aliphatic carbons were present in the expected regions.

X-band EPR spectra of the Cu(II) complexes were recorded at liquid nitrogen temperature in DMF solution. All the complexes showed well resolved quartet hyperfine splitting typical of square planar Cu(II) system (Fig. 1) which was confirmed by single crystal XRD technique. The frozen solution EPR spectra of the complexes are axial with $g_{\|} > g\perp > 2.00$ and the trend in the g value ($g_{\|} > g\perp > 2.00$) suggests that the unpaired electron in Cu(II) ion resides in d_{x2-y2} orbital. The observed values (Table 1) of $g_{\|}$ (2.16−2.21) and $A_{\|}$ (∼161-180) $\times 10^{-4}$ cm^{-1} for **1**−**5** are consistent with the presence of a square-based geometry as evident from the crystal structure of **1** and **2**. This is also supported by the value of $g_{\|}/A_{\|}$ quotient which fall within the range expected for square planar geometry (121−137 cm).[37]

2.2 Single crystal X-ray crystallographic studies

Thermal ellipsoid plots of the ligands (L1–L5) and the complexes (**1** and **2**) with the atomic labelling scheme are shown in Figs. 2-8. Crystal data and selected inter atomic bond lengths and angles are given in Tables 2-5. Suitable crystals of the ligands were grown by slow evaporation of ethanol solutions of the ligands. The crystal structure of the ligands shows the existence of intra and intermolecular hydrogen bonding between carbonyl oxygen and amino nitrogen. There exists a Y-aromaticity in guanidine moiety as C–N bond length varies between 1.3281-1.3595 Å (L1), 1.3358-1.3438 Å (L2), 1.3313-1.3526 Å (L3), 1.3387-1.3470 Å (L4) and 1.3352-1.3570 Å (L5).

Complexes **1** and **2** crystallized in triclinic *P-1* space group with Z of 1. The X-ray diffraction structure of complexes **1** and **2** reveals a perfect square planar geometry with oxygen and nitrogen atoms coordinate to Cu ion in a *trans* fashion. The perfect square planar geometry is also reflected by τ_4 parameter. τ_4 is the parameter used to describe the four coordinate system and it is used to determine the tetrahedral/square planar distortion. This term was coined by Dunitz and coworkers[38], and more recently by Keinan and Avnir.[39] τ_4 can be calculated using the formula $\tau_4 = [360° - (\alpha + ß)]/141°$. The value of τ_4 range from 1.00 for a perfect tetrahedral geometry, since 360 − 2(109.5) = 141, to zero for a perfect square planar

geometry, since 360−2(180) = 0. For the intermediate structure like trigonal pyramidal, τ_4 fall within the range of 0 to 1.00. In complexes **1** and **2**, the angle between O(1)-Cu(1)-O(1)#1 and N(1)#1-Cu(1)-N(1) is 180 ° which shows perfect square planar geometry. There is an increase in the C–O bond length and decrease in the C–N bond length (involved in coordination) in **1** and **2** compared to L1 and L2, respectively.

2.3 DNA binding studies

2.3.1 Electronic absorption titration

The interaction of copper(II) complexes with CT DNA was investigated using UV-Visible absorption studies. The electronic spectra of Cu(II) complexes (**1-5**) exhibited a band around 240-271 nm which corresponds to intraligand transition. The observation of changes in this band upon incremental addition of DNA was mostly used method to find out the binding constant. In general, a compound that binds to DNA through intercalation results in hypochromism and bathochromism due to strong stacking interaction between an aromatic chromophore and the base pairs of DNA. The interaction of complexes (**1-5**) was confirmed by the observed hypochromism with red shift (Fig. 9 and Fig. S1). The magnitude of hypochromism is in the order of **3**>**1**>**2**>**4**>**5**, which reflects the DNA binding affinities of the complexes. The intrinsic binding constant K_b was obtained from the ratio of slope to intercept in the plot of [DNA]/($\varepsilon_a - \varepsilon_f$) *versus* [DNA] according to the equation[40] [DNA]/($\varepsilon_a - \varepsilon_f$) = [DNA]/($\varepsilon_b - \varepsilon_f$) + 1/$K_b$ ($\varepsilon_b - \varepsilon_f$) where [DNA] is the concentration of DNA in base pairs, ε_a is the apparent extinction coefficient value found by calculating A(observed)/[complex], ε_f is the extinction coefficient for the free compound, and ε_b is the extinction coefficient for the compound in the fully bound form. Each set of data, when fitted into the above equation, gave a straight line with a slope of 1/($\varepsilon_b - \varepsilon_f$) and an y-intercept of 1/K_b($\varepsilon_b - \varepsilon_f$) and the value of K_b was determined from the ratio of slope to intercept (Fig. 11). The magnitudes of intrinsic binding constants (K_b) are given in Table 6. The K_b values were found to be in the range of 1.62 $\times 10^4$ - 1.63 $\times 10^5$ M^{-1}. The high binding ability of complex **3** compared to the other complexes is due to the presence of ethoxy group in guanidine ligand. The same is not observed in the case of complex **4** eventhough methoxy group is present. The reason for this may be due to the steric effect of the methoxy group which is present at the *ortho* position.

2.3.2 Ethidium bromide displacement studies

Fluorescence property has not been observed for the complexes at room temperature in solution or in the presence of CT DNA. So the binding of the complexes with DNA could not be directly predicted through the emission spectra. Hence, competitive binding study was

done to understand the mode of DNA interaction with the complexes.[41-43] Ethidium bromide (EB) is one of the most sensitive fluorescence probes that can bind with DNA.[44] The fluorescence of EB increases after intercalating into DNA. If the metal complex intercalates into DNA, it leads to a decrease in the binding sites of DNA available for EB, resulting in decrease in the fluorescence intensity of the CT DNA-EB system.[45] The extent of decrease in the fluorescence intensity (quenching) of CT DNA-EB reflects the extent of interaction of the complex with CT DNA. On adding Cu(II) complexes (0-50 μM) to CT DNA-EB, the quenching in the emission of DNA bound EB takes place (Fig. 10 and Fig. S2). Fluorescence quenching is explained by the Stern-Volmer equation[46] $F^o/F = 1 + K_q$ [Q] where F^o and F are the fluorescence intensities in the absence and presence of complex respectively, K_q is a linear Stern-Volmer quenching constant, and [Q] is the concentration of complex. The slope of the plot of F^o/F *versus* [Q] gave K_q (Fig. 12). The apparent DNA binding constant (K_{app}) values were calculated by using the equation K_{EB} [EB] = K_{app} [complex] where [complex] is the complex concentration at 50% reduction in the fluorescence intensity of EB, $K_{EB} = 1.0 \times 10^7$ M^{-1} and [EB] = 5 μM. K_q and K_{app} values are listed in Table 6.

2.4 DNA cleavage

To explore the DNA cleavage ability of complexes **1**-**5**, supercoiled (SC) pBR 322 DNA (40 μM in base pairs) was incubated at 37 ℃ with the complexes (100 μM) in a 5% DMF/5 mM Tris-HCl/50 mM NaCl buffer at pH 7.2 for 4 h in the absence of external agent. Complexes **3**-**5** cleave SC (Form I) DNA into nicked circular (NC) (Form II) DNA [Figure 13(A)], and the DNA cleavage efficiency follows the order **5** (73.7%) > **3** (50.8%) > **4** (38.2%). Complexes **1** and **2** did not show any appreciable cleavage at the concentration of 100 μM. When increasing the concentration of complexes **1** and **2** (200 μM), DNA cleavage occurs with the percentage of 31.5 and 31.9 respectively [Fig. 13(B)]. The study reveals that **5** cleaves DNA more efficiently than the other complexes, because of the strong partial intercalation of the extended aromatic ring of the naphthyl group.[47]

2.5 Molecular docking study

2.5.1 Molecular docking with DNA

Molecular docking is an important *in-silico* computational tool for the rational design of new chemotherapeutic drugs, which predicts non-covalent interaction between the drug molecules and the nucleic acids of DNA. Conformation of docked complexes was analyzed in terms of energy, hydrogen bonding, and hydrophobic interaction between complexes and DNA. From the docking scores, the free energy of binding (FEB) of the complexes was calculated and

details are shown in Table 7.

Molecular docking experiment reveals that the docked complexes fit into the DNA comfortably involving van der Waals interaction, hydrophobic and hydrogen bonding contacts with DNA functional groups without disrupting the double helical structure of DNA, resulted in the binding energy between -5.71 and -8.88 kcal/mol. Complex **1** shows higher binding energy of -8.88 kcal/mol. Figure 14 shows the docked models.

2.5.2 Molecular docking with human DNA topoisomerase I

All the copper(II) complexes were subjected to molecular docking with human DNA topoisomerase I using the AutoDock Tools (ADT) version 1.5.6 and AutoDock version 4.2.5.1. The X-ray crystallographic structure of the human DNA Topoisomerase I complex (PDB ID: 1SC7) was retrieved from Protein Data Bank, in which Topo I is bound to the oligonucleotide sequence 50-AAAAAGACTTsX-GAAAATTTTT-30 where 's' is 50-bridging phosphorothiolate of the cleaved strand and 'X' represents any of the four bases A, G, C or T. The SH of G11 on the scissile strand was changed to OH and phosphoester bond of G12 in 1SC7 was rebuilt.[48]

Docked ligand conformation was analyzed in terms of energy, hydrogen bonding, and hydrophobic interaction between ligand and DNA Topoisomerase I. The free energy of binding (FEB) of the compound was calculated from docking scores and details are given in Table 8. The molecular docking results revealed that all the copper(II) complexes approach towards the DNA cleavage site in the DNA-Topoisomerase I forming a stable complex through non-covalent interactions like hydrogen bonding, hydrophobic and van der Waals interactions, results in the binding energy value of -10.42 to -12.05 kcal/mol, subsequently leading to inhibitory effect on DNA Topoisomerase I.

Molecular docking results of DNA-Topoisomerase I with the copper complexes show that **5** binds efficiently with the DNA-Topoisomerase I receptor and exhibits very high free energy of binding (-12.05 kcal/mol). The high binding energy of **5** may due to the presence of the naphthyl moiety. The order of binding affinity of the complexes with DNA Topoisomerase I receptor is **5**>**1**>**4**>**3**>**2**. Docking studies reveal that the benzyl N–H and nitrogen attached to aromatic group exhibit polar interactions with C=O of DT–10 residue, and another benzyl N–H and imine nitrogen exhibit polar interactions with C=O of TGP–11 residue. Besides these polar interactions, a π–π interaction has been observed between aromatic ring in the complex and ring of TGP–11 residue. Interaction of the copper(II) complexes with the DNA Topoisomerase I receptor is shown in Figure 15.

Molecular docking studies of the copper(II) complexes with the DNA Topoisomerase I receptor revealed that all the docked complexes bind more efficiently suggesting that they can be a potential scaffold to be used for therapeutic purpose. In addition to this, DNA intercalating forces with the active site residues of the protein or to the base pairs of DNA, play a vital role in the inhibition of the targeting receptor.[49] Interestingly, the complexes occupy the topoisomerase binding site which may suppress the association of topoisomerase with DNA, thus forming more stable complex with DNA, which results in the topoisomerase inhibition activity and can be the promising DNA targeting anticancer drugs.

2.6 Protein binding studies

2.6.1 Absorbance and fluorescence studies

The interaction of complexes with BSA was investigated using fluorescence studies. BSA (1 μM) was titrated with various concentrations of the complexes (0–20 μM). Fluorescence spectra were recorded in the range of 290-500 nm upon excitation at 280 nm. The changes observed on the fluorescence emission spectra of BSA on addition of increasing concentration of the copper(II) complexes are shown in Figs. 16 and S3. On the addition of complexes **1**-**5** to BSA**,** there is a significant decrease in the fluorescence intensity of BSA at 346 nm upto 77.19, 83.22, 81.78, 80.08 and 88.41% with blue shift of 11, 11, 14, 8 and 8 nm respectively. The decrease in fluorescence intensity with blue shift shows the interaction between the complexes and BSA.[50,51] The fluorescence quenching is described by the Stern–Volmer relation $F°/F = 1 + K_q[Q]$ where F^o and F demonstrate the fluorescence intensities in the absence and presence of quencher, respectively, K_q is a linear Stern–Volmer quenching constant, and [Q] is the quencher concentration. The quenching constant (K_q) can be calculated from the plot of F^o/F *versus* [Q] (Fig. 18). When small molecules bind independently to a set of equivalent site, on a macromolecule, the equilibrium between free and bound molecules is represented by the Scatchard equation[52, 53] $\log[(F^o - F)/F] = \log K_b + n \log[Q]$ where K_b is the binding constant of the complex with BSA and n is the number of binding sites. From the plot of $\log[(F^o - F)/F]$ *versus* log[Q] (Fig. 19), the number of binding sites (n) and the binding constant (K_b) values have been obtained. K_q, K_b and n values for the interaction of the copper(II) complexes with BSA are provided in Table 9. The calculated value of n is around 0.7 to 1 for the complexes, proving the existence of single binding site in BSA for all of the complexes. From the values of K_q and K_b, it is proved that complex **5** interacts with BSA more strongly than the rest of the complexes. Surprisingly the complex which interacts weakly with CT DNA, binds strongly with BSA.[54]

Quenching usually occurs either by dynamic or static mode. Dynamic quenching is a process in which the fluorophore and the quencher come into contact during the transient existence of the excited state. On the other hand, static quenching refers to the formation of a fluorophore–quencher complex in the ground state.[55] UV-Visible absorption spectroscopy is the tool to determine the type of quenching involved. Addition of the complexes to BSA lead to an increase in BSA absorption intensity without affecting the position of absorption band (Fig. 17). It showed the existence of static interaction between BSA and the complexes.

2.6.2 Characteristics of synchronous fluorescence spectra

Synchronous fluorescence spectroscopy can give valuable information on the microenvironment near different fluorophores, and the difference between the emission and excitation wavelengths (Δλ) reflects the spectra of different fluorophores.[56] Tyrosine, tryptophan and phenylalanine residues are responsible for the fluorescence property of BSA. In this experiment, synchronous fluorescence spectra of BSA in the absence and presence of increasing concentrations (2–20 μM) of **1-5** were obtained at different Δλ. At Δλ = 15 nm, the synchronous spectrum of BSA is characteristic of tyrosine while the corresponding spectrum at Δλ = 60 nm is characteristic of tryptophan.[56-59] On addition of the complexes, the fluorescence intensity of tyrosine residue at 300 nm decreased in the magnitude of 57.6, 68.1, 66.8, 59.7 and 82.6% with 2, 3, 1, 5, 5 nm red shift for complexes **1-5** respectively (Figs. 20 and S4). Similarly, there was also decrease in the intensity of tryptophan residue at 340 nm. The magnitude of decrease was 77.8, 83.5, 81.19, 80.9 and 88.1% with 3, 4, 1, 2, 3 nm red shift for complexes **1-5** respectively (Figs. 21 and S5). The synchronous fluorescence spectra clearly suggested that the fluorescence intensity of both the tryptophan and tyrosine was affected with increasing concentration of the complexes. The results indicate that the interaction of complexes with BSA affects the conformation of both tryptophan and tyrosine micro-regions.

2.7 Superoxide scavenging study

The superoxide dismutase (SOD) activity of the complexes was investigated by NBT assay. Several complexes containing transition metals[60] including copper, are known to mimic SOD, although their structures are totally unrelated to the native enzyme.[61] The percentage inhibition of formazan formation at various concentrations of complexes was measured by measuring the absorbance at 560 nm and plotted to a straight line. As the concentration of tested complexes was increased, the slope (*m*) was decreased. Percentage inhibition of the reduction of NBT was plotted against the concentration of the complexes (Fig. 22). The

complexes exhibited SOD-like activity at biological pH with the IC_{50} values in the range of 1.53–5.62 μM. The superoxide scavenging data are shown in Table 10. Even though the SOD-mimetic complexes obtained were not as effective as the enzyme (bovine erythrocyte SOD, $IC_{50} = 2.1 \times 10^{-7}$ M; horseradish SOD, $IC_{50} = 7.0 \times 10^{-8}$ M)[62,63], their experimental IC_{50} values were below 20.0×10^{-6} M, so our complexes can be considered as active SOD mimetics.[64, 65]

2.8 Cytotoxicity

The *in vitro* cytotoxic activity of the complexes (**1**-**5**) was carried out against human breast (MCF7), lung (A549) cancer and mouse embryonic fibroblasts (NIH 3T3) cell lines using MTT assay.[66] Figs. 23, 24 and S6 show the cytotoxicity of the complexes (**1**-**5**) after 24 h incubation on MCF7, A549 and NIH 3T3 cell lines respectively. Complexes were dissolved in DMSO and blank sample containing the same volume of DMSO was taken as control to identify the activity of the solvent in this experiment. Cyclophosphamide was used as a positive control to assess the cytotoxicity of the tested complexes. The results were analyzed by means of cell inhibition expressed as IC_{50} values and are shown in Table 11. The IC_{50} values show that complex **3** exhibited higher inhibitory effect than that of the other complexes and the IC_{50} is very close to the value of cyclophosphamide. Complex **1** also shows lower IC_{50} value with good cytotoxic effect. The rest of the complexes **2**, **4** and **5** show only moderate cytotoxicity. Fortunately all the complexes were less toxic towards the normal cell as it was evident from the higher IC_{50} values (above 550 μM). The cytotoxicity results are in good agreement with DNA binding ability of the complexes.

3. Experimental section

3.1 Materials and methods

Analytical grade reagents and chemicals (> 95% purity) were purchased from Sigma Aldrich / Merck and used as received. Solvents were purified according to the standard procedures. The melting points were determined on Lab India instrument and are uncorrected. The elemental analyses were performed using a Vario EL−III CHNS analyzer. FT-IR spectra were obtained as KBr pellets using a Nicolet-iS5 spectrophotometer. UV-Visible spectra were recorded using a Shimadzu-2600 spectrophotometer. Emission spectra were measured on a Jasco V-630 spectrofluorometer using 5% DMF in buffer as the solvent. NMR spectra were recorded in $CDCl_3$ by using TMS as an internal standard on a Bruker 500 MHz spectrometer. EPR spectra were recorded on a JEOL EPR spectrometer at liquid nitrogen temperature operating at X-band frequency (9.1 GHz).

3.2 Synthesis of *N, N′, N″*-trisubstituted guanidines

The guanidine ligands were synthesized from *N*-benzoyl-*N′*-benzylthiourea by a guanylation method. The thiourea was mixed with the desired substituted amine in DMF in an equimolar ratio with two equivalents of triethylamine. The temperature was maintained below 5 ℃ using an ice bath and one equivalent of mercuric chloride was added to the reaction mixture with vigorous stirring. The ice bath was removed after 30 minutes, while the stirring continued overnight. The progress of the reaction was monitored using TLC until all the thiourea was consumed. 20 mL of chloroform was added to the reaction mixture and the suspension was filtered through a celite bed to remove the HgS residue. The solvent was evaporated under reduced pressure and the solid residue was dissolved in 20 mL of CH_2Cl_2, then washed with water and the organic phase was dried over anhydrous Na_2SO_4. The residue obtained after evaporation of the solvent was recrystallized from ethanol to get crystals of the title compounds.

3.2.1 *N*-benzyl-*N′*-phenyl-*N″*-benzoylguanidine (L1)

N-benzoyl-*N′*-benzylthiourea (1.3517 g, 5 mmol), aniline (0.456 mL, 5 mmol) triethylamine (1 mL, 10 mmol) and $HgCl_2$ (1.3576 g, 5 mmol) were used. Yield: 82%. Colourless solid. M.p.: 101 ℃. UV−Vis (5% $CHCl_3$): λ_{max}, nm (ε, $dm^3mol^{-1}cm^{-1}$) 245 (19100), 273 (26900). FT-IR (KBR, ν cm^{-1}): 3414, 3174 (N–H), 1599 (C=O), 1568 (C=N). ^{1}H NMR (500 MHz, $CDCl_3$): δ, ppm 4.78 (s, 2H), 5.25 (s, 1H), 7.24-7.46 (m, 13H), 8.26-8.27 (d, *J* = 7 Hz, 2H), 12.19 (s, 1H). ^{13}C NMR (125 MHz, $CDCl_3$): δ, ppm 45.2 (aliphatic CH_2), 125.5, 126.9, 127.5, 127.6, 127.8, 128.8, 129.1, 130.0, 131.2, 136.0, 138.5 (aromatic C), 158.7 (C=N), 177.8 (C=O). HRMS Calcd for $C_{21}H_{19}N_3O$: 329.1528 Found: 329.1523.

3.2.2 *N*-benzyl-*N′*-(4-methylphenyl)-*N″*-benzoylguanidine (L2)

N-benzoyl-*N′*-benzylthiourea (1.3517 g, 5 mmol), 4-methylaniline (0.5357 g, 5 mmol), triethylamine (1 mL, 10 mmol) and $HgCl_2$ (1.3576 g, 5 mmol) were used. Yield: 81%. Colourless solid. M.p.: 94 ℃. UV−Vis (5% $CHCl_3$): λ_{max}, nm (ε, $dm^3mol^{-1}cm^{-1}$) 235 (13500), 272 (22600). FT-IR (KBR): ν, cm^{-1} 3299, 3145 (N–H), 1594 (C=O), 1571 (C=N). ^{1}H NMR (500 MHz, $CDCl_3$) δ, ppm: 2.07 (s, 3H), 4.81-4.80 (d, *J* = 5.5 Hz, 2H), 5.22 (s, 1H), 7.17-7.50 (m, 12H), 8.29-8.30 (d, *J* = 7.5 Hz, 2H), 12.07 (s, 1H). ^{13}C NMR (125 MHz, $CDCl_3$): δ, ppm 20.9 (aliphatic CH_3), 45.2 (aliphatic CH_2), 125.7, 127.5, 127.8, 128.7, 129.1, 130.6, 131.1, 133.1, 137.0, 138.6 (aromatic C), 158.9 (C=N), 177.7 (C=O). HRMS Calcd for $C_{22}H_{21}N_3O$: 343.1685 Found: 343.1685.

3.2.3 *N*-benzyl-*N′*-(4-ethoxyphenyl)-*N″*-benzoylguanidine (L3)

N-benzoyl-*N′*-benzylthiourea (1.3517 g, 5 mmol), 4-ethoxyaniline (0.644 mL, 5 mmol), triethylamine (1 mL, 10 mmol) and $HgCl_2$ (1.3576 g, 5 mmol) were used. Yield: 79%. Colourless solid. M.p.: 141 ℃. UV−Vis (5% $CHCl_3$): λ_{max}, nm (ε, $dm^3mol^{-1}cm^{-1}$) 240 (35400), 271 (39600). FT-IR (KBR): ν, cm^{-1} 3419, 3192 (N–H), 1594 (C=O), 1567(C=N). ^{1}H NMR (500 MHz, $CDCl_3$): δ, ppm 1.42-1.45 (t, *J* = 7 Hz, 3H), 4.02-4.02-4.06 (q, 7 Hz, 2H), 4.78-4.80 (d, *J* = 5.5 Hz, 2H), 5.10 (s, 1H), 6.92-6.94 (dd, *J* = 2 Hz, 2 Hz, 2H), 7.21-7.48 (m, 10 H), 8.28-8.30 (d, *J* = 7.5 Hz, 2H), 11.93 (s, 1H). ^{13}C NMR (125 MHz, $CDCl_3$): δ, ppm 14.7 (aliphatic CH_3), 45.1 (aliphatic CH_2), 63.7 (aliphatic CH_2–O), 115.7, 127.5, 127.6, 127.8, 128.7, 129.1, 131.1, 138.6, 158.0 (aromatic C), 159.4 (C=N), 177.7 (C=O). HRMS Calcd for $C_{23}H_{23}N_3O_2$: 373.1790 Found: 373.1790.

3.2.4 *N*-Benzyl-*N′*-(2-methoxyphenyl)-*N″*-benzoylguanidine (L4)

N-benzoyl-*N′*-benzylthiourea (1.3517 g, 5 mmol), 2-methoxyaniline (0.564 mL, 5 mmol), triethylamine (1 mL, 10 mmol) and $HgCl_2$ (1.3576 g, 5 mmol) were used. Yield: 84%. Colourless solid. M.p.: 134 ℃. UV−Vis (5% $CHCl_3$): λ_{max}, nm (ε, $dm^3mol^{-1}cm^{-1}$) 237 (7900), 272 (12500), 290 (10800). FT-IR (KBR): ν, cm^{-1} 3285, 3165 (N–H), 1602 (C=O), 1561 (C=N). ^{1}H NMR (500 MHz, $CDCl_3$): δ, ppm 3.77 (s, 3H), 4.79 (s, 2H), 5.26 (s, 1H), 6.91-6.92 (d, *J* = 6 Hz, 1H), 6.95-6.98 (t, *J* = 7.5 Hz, 1H), 7.17-7.46 (m, 10H), 8.26-8.28 (d, *J* = 7.5 Hz, 2H), 11.96 (s, 1H). ^{13}C NMR (125 MHz, $CDCl_3$): δ, ppm 45.3 (aliphatic CH_2), 55.7 (aliphatic CH_3–O), 111.8, 121.0, 127.5, 127.8, 128.8, 129.2, 131.1, 138.7 (aromatic C), 158.7 (C=N), 177.7 (C=O). HRMS Calcd for $C_{22}H_{21}N_3O_2$: 359.1634 Found: 359.1639.

3.2.5 *N*-Benzyl-*N′*-naphthyl-*N″*-benzoylguanidine (L5)

N-benzoyl-*N′*-benzylthiourea (1.3517 g, 5 mmol), 1-naphthylamine (0.7159 g, 5 mmol), triethylamine (1 mL, 10 mmol) and $HgCl_2$ (1.3576 g, 5 mmol) were used. Yield: 70%. Colourless solid. M.p.: 116 ℃. UV−Vis (5% $CHCl_3$): λ_{max}, nm (ε, $dm^3mol^{-1}cm^{-1}$) 240 (28700), 273 (27700), 290 (26400). FT-IR (KBR): ν, cm^{-1} 3418, 3207 (N–H), 1591 (C=O), 1567 (C=N). ^{1}H NMR (500 MHz, $CDCl_3$): δ, ppm 4.79-4.80 (d, *J* = 5.5 Hz, 2H), 5.12 (s, 1H), 7.27-7.93 (m, 14 H), 8.15 (s, 1H), 8.36-8.37 (d, *J* = 7.5 Hz, 2H), 12.54 (s, 1H). ^{13}C NMR (125 MHz, $CDCl_3$): δ, ppm 45.1 (aliphatic CH_2), 122.8, 124.1, 125.6, 127.0, 127.3, 127.4, 127.9, 128.2, 128.4, 128.6, 129.2, 129.7, 131.2, 131.9, 134.7, 138.5 (aromatic C), 159.6 (C=N), 178.1 (C=O); HRMS Calcd for $C_{25}H_{21}N_3O$: 379.1685 Found: 379.1690.

3.3 Synthesis of copper(II) complexes (1-5)

A methanolic solution of copper acetate monohydrate was added into the methanolic solution of appropriate guanidine ligand. The reaction mixture was stirred for 6 h at room temperature. The solid product formed was filtered and washed with methanol. Suitable crystals of the complexes (**1** and **2**) were grown by vapour diffusion method using $CHCl_3$/n-hexane.

3.3.1 Bis(*N*-benzyl-*N′*-phenyl-*N″*-benzoylguanidinato)copper(II) (1)

L1 (0.3294 g, 1 mmol) and $Cu(CH_3COO)_2 \cdot H_2O$ (0.0998 g, 0.5 mmol) were used. Yield: 79%. Blue solid. M.p.: 210 ℃. Anal. Calcd. for $C_{42}H_{36}CuN_6O_2$ (720.32): C, 70.03; H, 5.04; N, 11.67. Found: C, 70.27; H, 5.12; N, 11.71. UV-Vis ($CHCl_3$): λ_{max}, nm (ε, $dm^3mol^{-1}cm^{-1}$) 219 (24100), 271 (45200), 388 (2400), 596 (72). FT-IR (KBR): ν, cm^{-1} 3421 (N–H), 1589 (C=O), 1552 (C=N). EPR (LNT): 'g' values 2.21, 2.04.

3.3.2 Bis(*N*-benzyl-*N′*-(4-methylphenyl)-*N″*-benzoylguanidinato)copper(II) (2)

L2 (0.3434 g, 1 mmol) and $Cu(CH_3COO)_2 \cdot H_2O$ (0.0998 g, 0.5 mmol) were used. Yield: 81%. Blue solid. M.p.: 211 ℃. Anal. Calcd. for $C_{44}H_{40}CuN_6O_2$ (748.37): C, 70.62; H, 5.39; N, 11.23. Found: C, 69.69; H, 5.16; N, 11.19. UV-Vis ($CHCl_3$): λ_{max}, nm (ε, $dm^3mol^{-1}cm^{-1}$) 271 (46800), 389 (3000), 615 (92). FT-IR (KBR): ν, cm^{-1} 3425 (N–H), 1590 (C=O), 1553 (C=N). EPR (LNT): 'g' values 2.16, 2.02.

3.3.3 Bis(*N*-benzyl-*N′*-(4-ethoxyphenyl)-*N″*-benzoylguanidinato)copper(II) (3)

L3 (0.3734 g, 1 mmol) and $Cu(CH_3COO)_2 \cdot H_2O$ (0.0998 g, 0.5 mmol) were used. Yield: 83%. Green solid. M.p.: 194 ℃. Anal. Calcd. for $C_{46}H_{44}CuN_6O_4$ (808.27): C, 68.34; H, 5.49; N, 10.40. Found: C, 69.04; H, 5.61; N, 10.40. UV-Vis ($CHCl_3$): λ_{max}, nm (ε, $dm^3mol^{-1}cm^{-1}$) 240 (65300), 271 (65800), 377 (3800), 601 (92). FT-IR (KBR): ν, cm^{-1} 3427 (N–H), 1590 (C=O), 1545 (C=N). EPR (LNT): 'g' values 2.20, 2.01.

3.3.4 Bis(*N*-benzyl-*N′*-(2-methoxyphenyl)-*N″*-benzoylguanidinato)copper(II) (4)

L4 (0.3594 g, 1 mmol) and $Cu(CH_3COO)_2 \cdot H_2O$ (0.0998 g, 0.5 mmol) were used. Yield: 79%. Light blue solid. M.p.: 178 ℃. Anal. Calcd. for $C_{44}H_{40}CuN_6O_4$ (780.37): C, 67.72; H, 5.17; N, 10.77. Found: C, 67.50; H, 5.08; N, 11.19. UV-Vis ($CHCl_3$): λ_{max}, nm (ε, $dm^3mol^{-1}cm^{-1}$) 271 (46800), 389 (3000), 615 (92). FT-IR (KBR): ν, cm^{-1} 3425 (N–H), 1590 (C=O), 1553 (C=N). EPR (LNT): 'g' values 2.2105, 2.024.

3.3.5 Bis(*N*-benzyl-*N′*-naphthyl-*N″*-benzoylguanidinato)copper(II) (5)

L5 (0.3794 g, 1 mmol) and $Cu(CH_3COO)_2 \cdot H_2O$ (0.0998 g, 0.5 mmol) were used. Yield: 81%. Green solid. M.p.: 224 ℃. Anal. Calcd. for $C_{50}H_{40}CuN_6O_2$ (820.43): C, 73.20; H, 4.91; N, 10.24. Found: C, 72.94; H, 4.89; N, 10.17. UV-Vis ($CHCl_3$): λ_{max}, nm (ε, $dm^3mol^{-1}cm^{-1}$) 240

(37000), 271(37700), 592 (104). FT-IR (KBR): ν, cm^{-1} 3429 (N–H), 1588 (C=O), 1547 (C=N). EPR (LNT): 'g' values 2.21, 2.02.

3.4 Single crystal X-ray diffraction studies

A Bruker APEX2 (Mo Kα) or Bruker GADDS (Cu Kα) X-ray (three-circle) diffractometer was employed for crystal screening, unit cell determination, and data collection. Integrated intensity information for each reflection was obtained by reduction of the data frames with the program APEX2.[67] The integration method employed a three dimensional profiling algorithm and all data were corrected for Lorentz and polarization factors, as well as for crystal decay effects. Finally, the data were merged and scaled to produce a suitable data set. The absorption correction program SADABS[68] was employed to correct the data for absorption effects. Systematic reflection conditions and statistical tests of the data suggested the space group (Tables 2, 3). Solution were obtained readily using SHELXTL (XS).[69] Hydrogen atoms were placed in idealized positions and were set riding on the respective parent atoms. All non-hydrogen atoms were refined with anisotropic thermal parameters. The structures were refined (weighted least squares refinement on F^2) to convergence.[69, 70] Olex2 was employed for the final data presentation and structure plots.[70]

3.5 DNA binding studies

The DNA binding experiments were performed in Tris-HCl/NaCl buffer (50 mM Tris HCl/1 mM NaCl buffer, pH 7.2) using DMF (10%) solutions of the complexes. The concentration of CT DNA was determined from the absorption intensity at 260 nm with ε value[71] of 6600 M^{-1} cm^{-1}. Absorption titration experiments were made using different concentrations of CT DNA, while keeping the complex concentration as constant. Samples were equilibrated before recording each spectrum. The concentration of the complex used was 15 μM; CT DNA of varying concentration (5–40 μM) was added each time and the significant absorbance change was noted.

The competitive binding of each complex with EB has been investigated by fluorescence spectroscopic technique in order to examine whether the complex can displace EB from its CT DNA-EB complex. Ethidium bromide solution was prepared using Tris HCl/NaCl buffer (pH 7.2). The test solution was added in aliquots of 5 μM concentration to DNA-EB and the change in fluorescence intensity at 596 nm (450 nm excitation) was noted down.

3.6 DNA cleavage studies

A mixture of Tris buffer (5 mM Tris-HCl/50 mM NaCl buffer, pH 7.2), pBR 322 plasmid DNA (350 μg/mL) and complexes (**1**-**5**) were incubated for 4 h at 37 ℃. A dye solution (0.05% bromophenol blue and 5% glycerol) was added to the reaction mixture prior to electrophoresis. The samples were then analyzed by 1.5% agarose gel electrophoresis [Tris-HCl/Boric acid/EDTA (TBE) buffer, pH 8.0] for 2 h at 60 mV. The gel was stained with 0.5 μg mL^{-1} ethidium bromide, visualized by UV light and photographed. The extent of cleavage of the pBR 322 DNA was determined by measuring the intensities of the bands using AlphaImager HP instrument.

3.7 Molecular docking studies

The X-ray crystal structure of B-DNA (PDB ID: 1BNA) dodecamer $d(CGCGAATTCGCG)_2$ and human DNA Topo-I complex (PDB ID: 1SC7) were obtained from the Protein Data Bank (http://www.rcsb.org/pdb). 2D structure of copper complexes was drawn using ChemDraw Ultra 12.0 (ChemOffice 2010). Chem3D Ultra 12.0 was used to convert 2D structure into 3D and the energy was minimized using semi-empirical AM1 method. Molecular docking studies have been done using the AutoDock Tools (ADT) version 1.5.6 and AutoDock version 4.2.5.1 docking program.[72] The energy calculations were made using genetic algorithms. The outputs were exported to PyMol for visual inspection of the binding modes and for possible polar and hydrophobic interactions of the complexes with DNA.

3.8 Protein binding studies

The binding of copper(II) complexes (**1**-**5**) with BSA was studied using fluorescence spectra recorded at a fixed excitation wavelength of 280 nm and monitoring the emission at 335 nm. The excitation and emission slit widths and scan rates were constantly maintained for all the experiments. Stock solution of BSA was prepared in 50 mM phosphate buffer (pH 7.2) and stored in the dark at 4 ℃ for further use. Concentrated stock solutions of each test compound were prepared by dissolving them in DMF-phosphate buffer (5:95) and diluted with phosphate buffer to get required concentrations. 2.5 mL of BSA solution was titrated by successive additions of a 10^{-6} M stock solution of the complexes using a micropipette. For synchronous fluorescence spectra measurements, the same concentration of BSA and the complexes were used and the spectra were measured at two different Δλ values of 15 and 60 nm.

3.9 Superoxide scavenging study

The superoxide (O_2^-) radical scavenging assay was done based on the ability of the complexes to inhibit formazan formation by scavenging the superoxide radicals generated in

the riboflavin-light-NBT system.[73] Each 3 mL reaction mixture contained 50 mM sodium phosphate buffer (pH 7.6), 20 mg riboflavin, 10 mM methionine and 0.1 mg NBT. The reaction was started by illuminating the reaction mixture with different concentrations of the test complexes (2-10 μM) for 90 s. After illumination, the absorbance was measured at 560 nm immediately. The entire reaction assembly was enclosed in a box lined with aluminum foil. The above reaction mixture without test sample was used as the control. All the tests were run in triplicate and various concentrations of the complexes were used to fix the concentration range at which complexes showed around 50% activity. The percentage activity was calculated using the formula $[(A_0 - A_C)/A_0] \times 100$, where A_0 and A_C are the absorbance in the absence and presence of the tested complex respectively.

3.10 *In vitro* cytotoxicity evaluation by MTT assay

Cytotoxicity of the copper(II) complexes was evaluated on human breast (MCF7) and lung cancer (A549) and mouse embryonic fibroblasts (NIH 3T3) cell lines which were obtained from National Centre for Cell Science, Pune, India. Cell viability was carried out using MTT assay method. The MCF7 and A549 cells were grown in Eagles minimum essential medium containing 10% fetal bovine serum (FBS) while NIH 3T3 fibroblasts were grown in Dulbeccos modified Eagles medium (DMEM) containing 10% FBS. For screening experiment, the cells were seeded into 96-well plates in 100 mL of respective medium containing 10% FBS, at plating density of 10,000 cells/well and incubated at 37 ℃ for 24 h prior to addition of the complexes. Complexes (**1**-**5**) dissolved in DMSO (10-500 μM) were seeded to the wells. Triplication was maintained, and the medium without the complexes served as the control. After 24 h, the wells were treated with 20 μL MTT [5 mg mL^{-1} phosphate buffered saline (PBS)] and incubated at 37 ℃ for 4 h. The medium with MTT was then removed separately and the formed formazan crystals were dissolved in 100 mL DMSO. The absorbance at 570 nm was measured using ELISA plate reader. The graph was plotted between percentage of cell inhibition and concentration of the complexes. IC_{50} values were calculated from the percentage of inhibition. The percentage of cell inhibition was determined using the formula, % inhibition = [mean OD of untreated cells (control)/mean OD of treated cells (control)] ×100.

4. Conclusions

Copper(II) complexes containing *N*,*N*′,*N*″-trisubstituted benzyl based guanidine ligands were synthesized and characterized by analytical, spectroscopic and single crystal X-ray diffraction studies with a view to evaluate their biological applications. The DNA and protein binding of the complexes were investigated using absorbance and fluorescence spectroscopic

techniques. The complexes bind reasonably well to DNA in the order of 10^4 M^{-1} through intercalation. DNA cleavage ability shows complex **5** have better cleaving ability compared to that of the other complexes. The protein binding ability of the complexes was examined by fluorescence spectroscopy. The superoxide radical scavenging assay results showed that all the complexes possess significant activity. In addition the *in vitro* cytotoxicity of the complexes **1**-**5** suggested that complexes **3** and **1** have better cytotoxic activity compared to that of the other complexes. The cytotoxic activity towards normal cells shows high IC_{50} value which reveals that the complexes are cytotoxic towards only cancerous cells and it did not affect the normal cells. Further docked models also confirmed the binding affinity of the complexes with DNA. There is a correlation between the DNA binding and cytotoxicity of the complexes proving the complexes **3** and **1** to be a better candidate as an anticancer drug. But studies like DNA cleavage and docking models proved that complex **5** to be a better candidate. As a conclusion further mechanistic studies have to be dealt in detail to understand the controversy prevailing regarding the DNA interactions with the complexes.

Acknowledgements

K. J. thanks DST for doctoral fellowship under DST-INSPIRE programme. R. K. gratefully acknowledges DST for the financial support. We thank Sophisticated Analytical Instrumentation facility (SAIF), Indian Institute of Technology - Madras and Indian Institute of Technology - Bombay for NMR and EPR analyses respectively. We thank Dr. T. Parimelazhagan, Bharathiar University for his help in carrying out the antioxidant study.

References

1. I. Kostova, *Recent Pat. Anti-Cancer Drug Discovery*, 2006, **1**, 1-22.

2. A. Kamal, R. Ramu, V. Tekumalla, G. B. R. Khanna, M. S. Barkume, A. S. Juvekar and S. M. Zingde, *Bioorg. Med.Chem*., 2007, **15**, 6868-6875.

3. D. Dreher and A. F. Junod, *Eur. J. Cancer*, 1996, **32**, 30-38.

4. W. J. Chen, P. Guo, J. Song, W. Cao and J. Bian, *Bioorg. Med. Chem. Lett*., 2006, **16**, 3582-3585.

5. B. P. Esposito and R. Najjar, *Coord. Chem. Rev*., 2002, **232**, 137-149.

6. T. M. Sielecki, J. F. Boylan, P. A. Benfield and G. L. Trainor, *J. Med. Chem*., 1999, **43**, 1-18.

7. Z. Zang, L. Jin, X. Qian, M. Wei, Y. Wang, J. Wang, Y. Yang, Q. Xu, Y. Xu and F. Liu, *ChemBioChem*., 2007, **8**,113-121.

8. P. K. M. Siu, D. L. Ma and C. M. Che, *Chem.Commun*., 2005, 1025-1027.

9. J. Chern, Y. Leu, S. Wang, R. Jou, S. Hsu, Y. Liaw and H. Lin, *J. Med. Chem*., 1997, **40**, 2276-2286.

10. Z. Brzozowski, F. Saczewski and M. Gdaniec, *Eur. J. Med. Chem*., 2002, **37**, 285-293.

11. A. V. Dolzhenko, B. J. Tan, A. V. Dolzhenko, G. N. C. Chiu and W. K. Chui, *J. Fluor. Chem*., 2008, **129**, 429-434.

12. G. Murtaza, A. Badshah, M. Said, H. Khan, A. Khan, S. Khan, S. Siddiq, M. I. Choudhary, J. Boudreau and F. G. Fontaine, *Dalton Trans*., 2011, **40**, 9202-9211.

13. P. J. Bailey and S. Pace, *Coord. Chem. Rev*., 2001, **214**, 91-141.

14. K. Jeyalakshmi, N. Selvakumaran, N. S. P. Bhuvanesh, A. Sreekanth and R. Karvembu, *RSC Adv*., 2014, **4**, 17179-17195.

15. H. B. Kraatz and N. M. Nolte, *Concepts and Models in Bioinorganic Chemistry*; Wiley-VCH: Weinheim, Germany, 2006.

16. S. J. Lippard and J. M. Berg, *Principles of Bioinorganic Chemistry*; University Science Books: Mill Valley, CA, 1994.

17. Z. H. Harris and J. D. Gitlin, *Am. J. Clin. Nutr*., 1996, **63**, 836S-841S.

18. P. U. Maheswari, S. Roy, H. D. Dulk, S. Barends, G. V. Wezel, B. Kozlevcar, P. Gamez and J. Reedijk, *J. Am. Chem. Soc*., 2006, **128**, 710-711.

19. J. D. Ranford, P. J. Sadler and D. A. Tocher, *J. Chem. Soc., Dalton Trans*., 1993, 3393-3399.

20. C. H. Ng, K. C. Kong, S. T. Von, P. Balraj, P. Jensen, E. Thirthagiri, H. Hamada and M. Chikira, *Dalton Trans*., 2008, **4**, 447-454.

21. A. Barve, A. Kumbhar, M. Bhat, B. Joshi, R. Butcher, U. Sonawane and R. Joshi, *Inorg. Chem*., 2009, **48**, 9120-9132.

22. C. Fernandes, G. L. Parrilha, J. A. Lessa, L. J. M. Santiago, M. M. Kanashiro, F. S. Boniolo, A. J. Bortoluzzi, N. V. Vugman, M. H. Herbstand and A. H. Jr. *Inorg. Chim. Acta*, 2006, **359**, 3167-3176.

23. B. C. Bales, T. Kodama, Y. N. Weledji, M. Pitie, B. Meunier and M. M. Greenberg, *Nucleic Acids Res*., 2005, **33**, 5371-5379.

24. L. Turecky, P. Kalina, E. Uhlikova, *Klin. Wochenschr*., 1984, **62**, 187-189.

25. D. Yoshida, Y. Ikeda and S. Takanawa, *J. Neurooncol*., 1993, **16**, 109-115.

26. D. H. Petering, *Met. Ions Biol. Syst*., 1980, **11**, 197-229.

27. F. A. French and E. J. Blanz Jr, *Cancer Res*., 1965, **25**, 1454-1458.

28. F. A. French and E. J. Blanz Jr, *Cancer Res*., 1966, **26**, 1638-1640.

29. P. M. May, D. R. Williams, *In Metal Ions in Biological Systems*; H. Sigel Ed, Marcel Dekker: New York, 1981; Vol 12.

30. P. M. May, D. R. Williams, *In Metal Ions in Biological Systems*; H. Sigel Ed, Marcel Dekker: New York, 1981; Vol. 13.

31. T. Miura, T, A. Hori-i, H. Mototani and H. Takeuchi, *Biochemistry*, 1999, **38**, 11560-11569.

32. G. Binzet, N. Kulcu, U. Florke, H. Arslan, *J. Coord. Chem*., 2009, **62**, 3454-3462.

33. D. A. Powell, P. D. Ramsden and R. A. Batey, *J. Org. Chem.*, 2003, **68**, 2300-2309.

34. S. Cunha, M. B. Costa, H. B. Napolitano, C. Lauriucci and I. Vecanto, *Tetrahedron*, 2001, **57**, 1671-1675.

35. J. G. Tojal, A. G. Orad, J. L. Serra, J. L. Pizarro, L. Lezama, M. I. Arriortua, T. Rojo, *J. Inorg. Biochem*., 1996, **75**, 45-54.

36. J. Binoy, C. James, I. H. Joe, V. S. Jayakumar, *J. Mol. Str*., 2006, **784**, 32-46.

37. R. Loganathan, S. Ramakrishnan, E. Suresh, A. Riyasdeen, M. A. Akbarsha and M. Palaniandavar, *Inorg. Chem*., 2012, **51**, 5512-5532.

38. P. Murrayrust, H. B. Burgi and J. D. Dunitz, *J. Am. Chem. Soc*., 1975, **97**, 921-922.

39. S. Keinan and D. Avnir, *J. Chem. Soc., Dalton Trans.*, 2001, 941-947.

40. A. M. Pyle, J. P. Rehmann, R. Meshoyrer, C. V. Kumar, N. J. Turro and J. K. Barton, *J. Am. Chem. Soc*., 1989, **111**, 3051-3058.

41. N. Chitrapriya, T. Sathiyakamatchi, M. Zeller, H. Lee and K. Natarajan, *Spectrochim. Acta Part A*, 2011, **81**, 128-134.

42. J. R. Lakowicz and G. Webber, *Biochemistry*, 1973, **12**, 4161-4170.

43. B. C. Baguley and M. Lebret, *Biochemistry*, 1984, **23**, 937-943.

44. E. Nyarko, N. Hanada, A. Habib and M. Tabata, *Inorg. Chim. Acta*, 2004, **357**, 739-745.

45. J. B. Lepecq and C. Paoletti, *J. Mol. Biol*., 1967, **27**, 87-106.

46. K. S. Ghosh, B. K. Sahoo, D. Jana and S. Dasgupta, *J. Inorg. Biochem*., 2008, **102**, 1711-1718.

47. S. Ramakrishnan, D. Shakthipriya, E. Suresh, V. S. Periasamy, M. A. Akbarsha, and M. Palaniandavar, *Inorg. Chem*., 2011, **50**, 6458–6471.

48. X. S. Xiao, S. Antony, Y. Pommier and M. Cushman, *J. Med. Chem*., 2005, **48**, 3231-3238.

49. X. S. Xiao and M. Cushman, *J. Am. Chem. Soc*., 2005, **127**, 9960-9961.

50. D. S. Raja, G. Paramaguru, N. S. P. Bhuvanesh, J. H. Reibenspies, R. Renganathan and K. Natarajan, *Dalton Trans*., 2011, **40**, 4548-4559.

51. D. S. Raja, N. S. P. Bhuvanesh and K. Natarajan, *Eur. J. Med.Chem*., 2011, **46**, 4584-4594.

52. J. R. Lakowicz, Fluorescence Quenching: Theory and Applications. Principles of Fluorescence Spectroscopy; Kluwer Academic/Plenum Publishers: New York, 1999; pp 53−127.

53. X. Z. Feng, Z. Yang, L. J. Wang, C. Bai, *Talanta*, 1998, **47**, 1223-1229.

54. V. Rajendiran, R. Karthik, M. Palaniandavar, H. S. Evans, V. S. Periasamy, M. A. Akbarsha, B. S. Srinag and H. Krishnamurthy, *Inorg. Chem*., 2007, **46**, 8208-8221.

55. M. Bhattacharyya, U. Chaudhuri and R. K. Poddar, *Biochem. Biophys. Res. Commun*., 1990, **167**, 1146-1153.

56. J. N. Miller, *Proc. Anal. Div. Chem. Soc*., 1979, **16**, 199-208.

57. C. X. Wang, F. F. Yan, Y. X. Zhang and L. Ye, *J. Photochem. Photobiol*., *A*, 2007, **192**, 23-28.

58. F. Zhang, Q. Y. Lin, S. K. Li, Y. L. Zhao, P. P. Wang and M. M. Chen, *Spectrochim. Acta, Part A*, 2012, **98**, 436-443.

59. W. C. Albert, W. M. Gregory and G. S. Allan, *Anal. Biochem*., 1993, **213**, 407-413.

60. R. Rajan, R. Rajaram, B. U. Nair, T. Ramasami and S. K. Mandal, *J. Chem. Soc., Dalton Trans*., 1996, 2019-2021.

61. U. Weser, L. M. Schubotz and E. Lengfelder, *J. Mol. Catal*., 1981, **13**, 249-261.

62. S. B. Etcheverry, E. G. Ferrer, L. Naso, J. Rivadeneira, V. Salinas and P. A. M. Williams, *J. Biol. Inorg. Chem*., 2008, **13**, 435-447.

63. I. Schepetkin, A. Potapov, A. Khlebnikov, E. Korotkova, G. A. Lukina, L. Malovichko, M. Kirpotina and T. Quinn, *J. Biol. Inorg. Chem*., 2006, **11**, 499-513.

64. N. A. Roberts and P. A. Robinson, *Br. J. Rheumatol*., 1985, **24**, 128-136.

65. E. G. Ferrer, N. Baeza, L. G. Naso, E. E. Castellano, O. E. Piro and P. A. M. Williams, *J. Trace Elem. Med. Biol*., 2010, **24**, 20-26.

66. M. Blagosklonny and W. S. EIdiery, *Int. J. Cancer*, 1996, **67**, 386-392.

67. APEX2 "*Program for Data Collection on Area Detectors*" BRUKER AXS Inc., 5465 East Cheryl Parkway, Madison, WI 53711-5373, USA.

68. SADABS, G. M. Sheldrick, "*Program for Absorption Correction of Area Detector Frames*", BRUKER AXS Inc., 5465 East Cheryl Parkway, Madison, WI 53711-5373, USA.

69. G. M. Sheldrick, *Acta Cryst*., 2008, **A64**, 112-122.

70. O. V. Dolomanov, L. J. Bourhis, R. J. Gildea, J. A. K. Howard and H. Puschmann, *J. Appl. Cryst*., 2009, **42**, 339-341.

71. M. E. Reichmann, S. A. Rice, C. A. Thomas and P. Doty, *J. Am. Chem. Soc.*, 1954, **76**, 3047-3057.

72. http://autodock.scripps.edu/resources/references

73. C. Beauchamp and I. Fridovich, *Anal. Biochem*., 1971, **44**, 276-287.

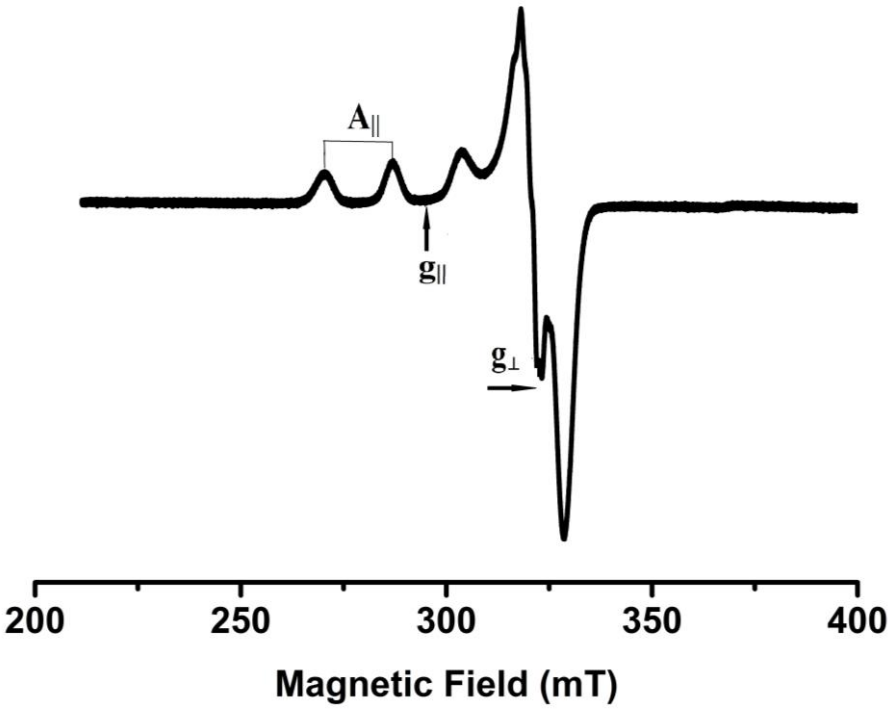

Fig. 1 EPR spectrum of complex **4** in frozen DMF solution.

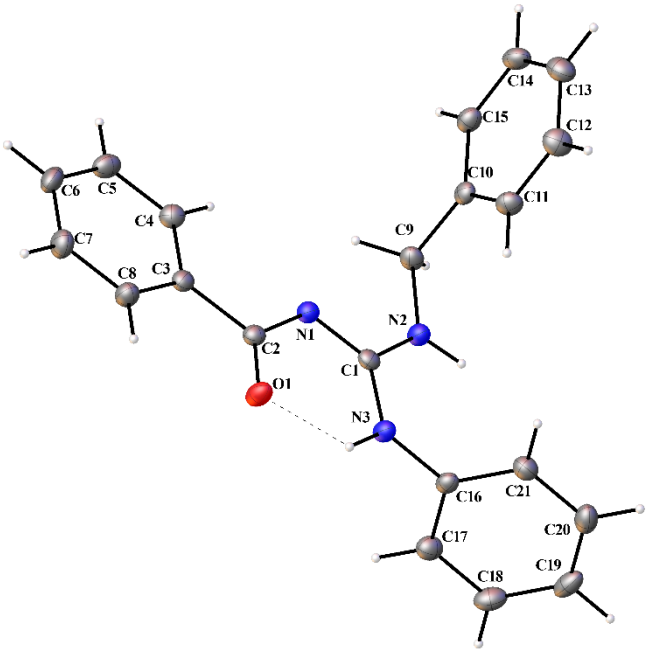

Fig. 2 Thermal ellipsoid plot of L1.

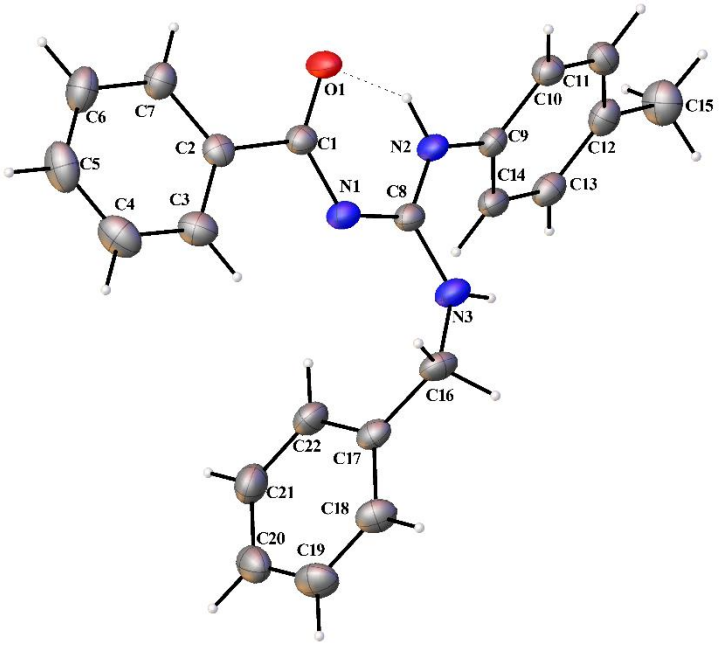

Fig. **3** Thermal ellipsoid plot of L2.

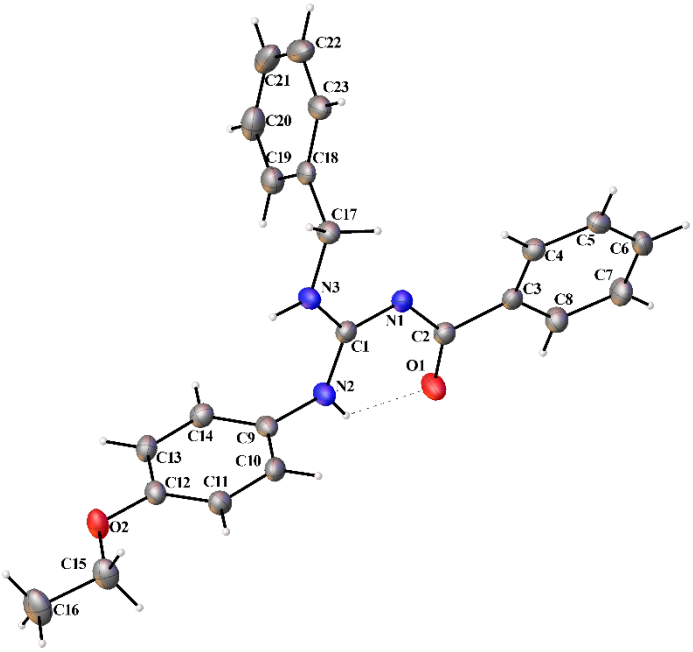

Fig. 4 Thermal ellipsoid plot of L3.

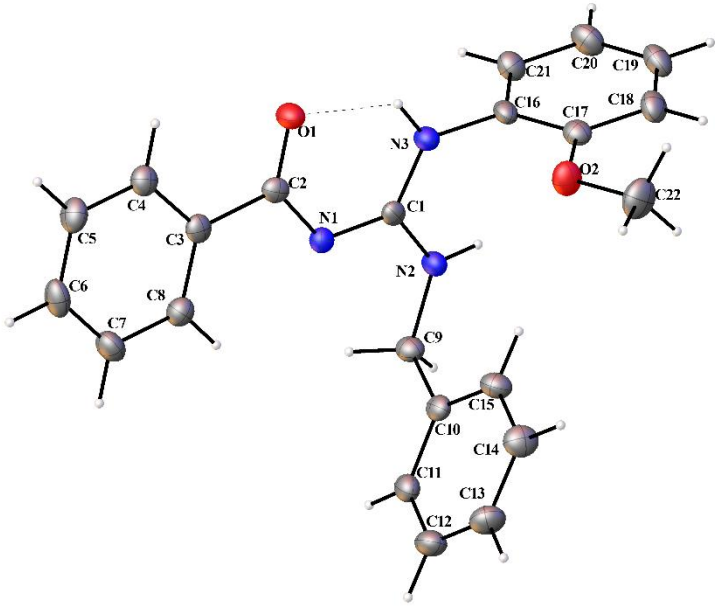

Fig. 5 Thermal ellipsoid plot of L4.

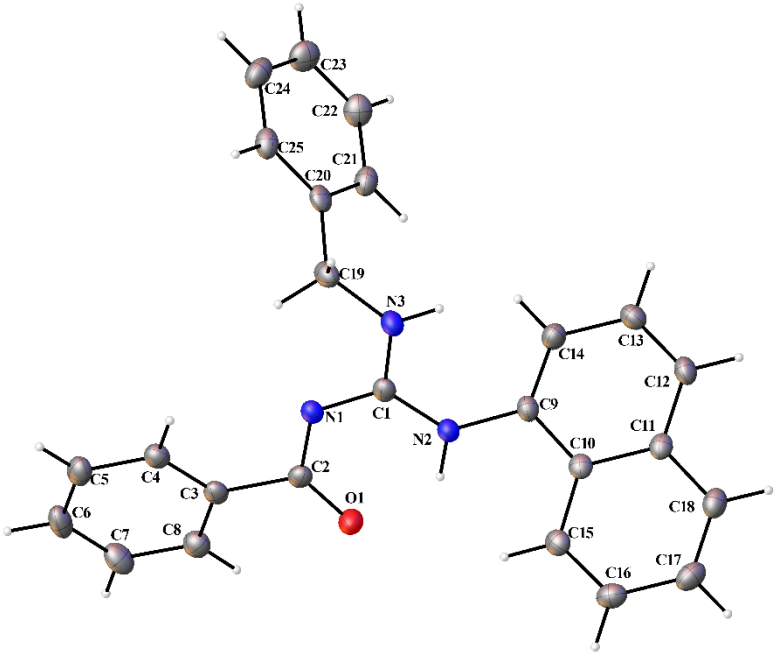

Fig. 6 Thermal ellipsoid plot of L5.

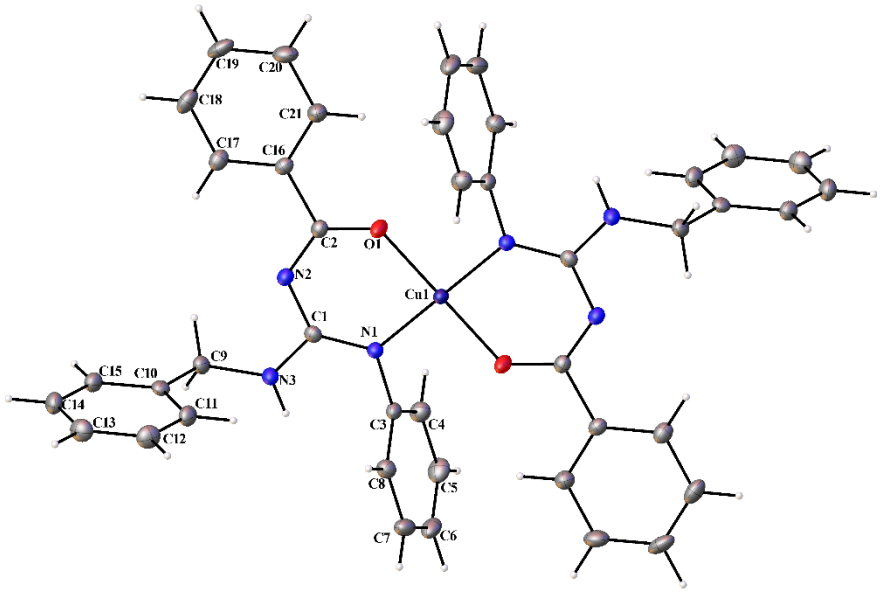

Fig. 7 Thermal ellipsoid plot of **1**.

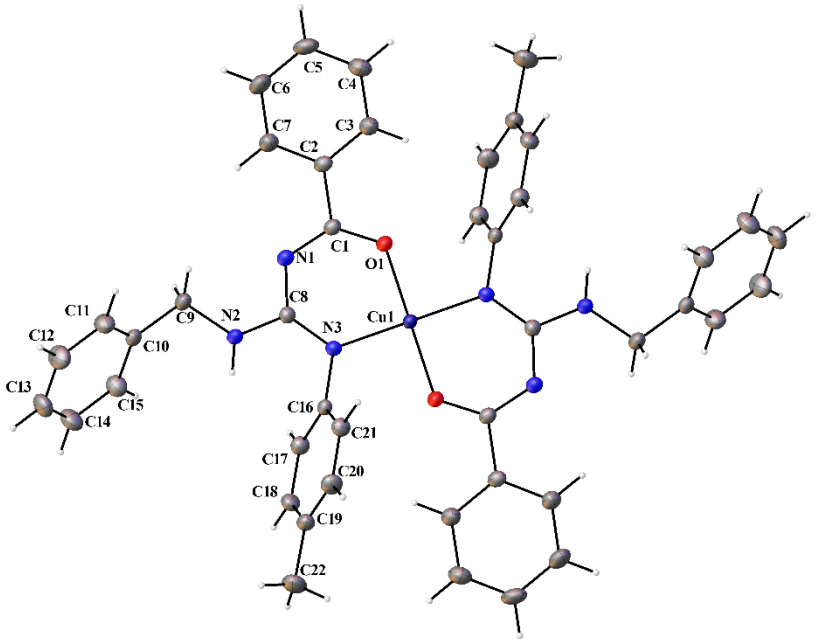

Fig. 8 Thermal ellipsoid plot of **2**.

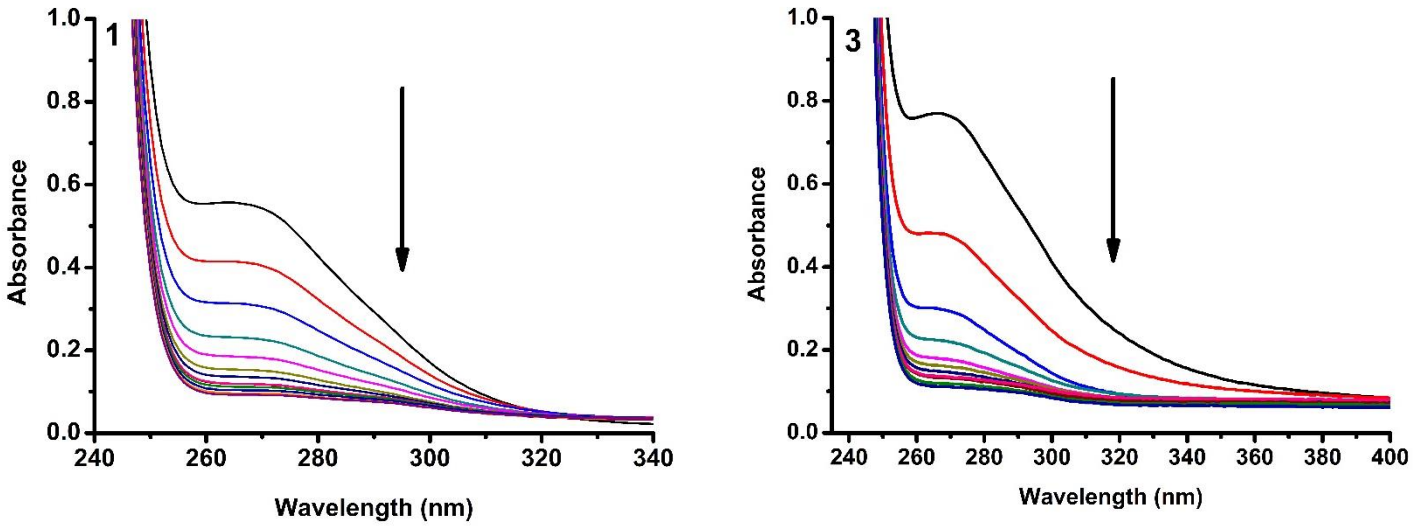

Fig. 9 Absorption spectra of complexes **1** and **3** in Tris-HCl buffer upon addition of CT DNA. [Complex] = 2.0 $\times 10^{-5}$ M, [DNA] = 0-40 μM. Arrow shows that the absorption intensity decreases upon increasing DNA concentration.

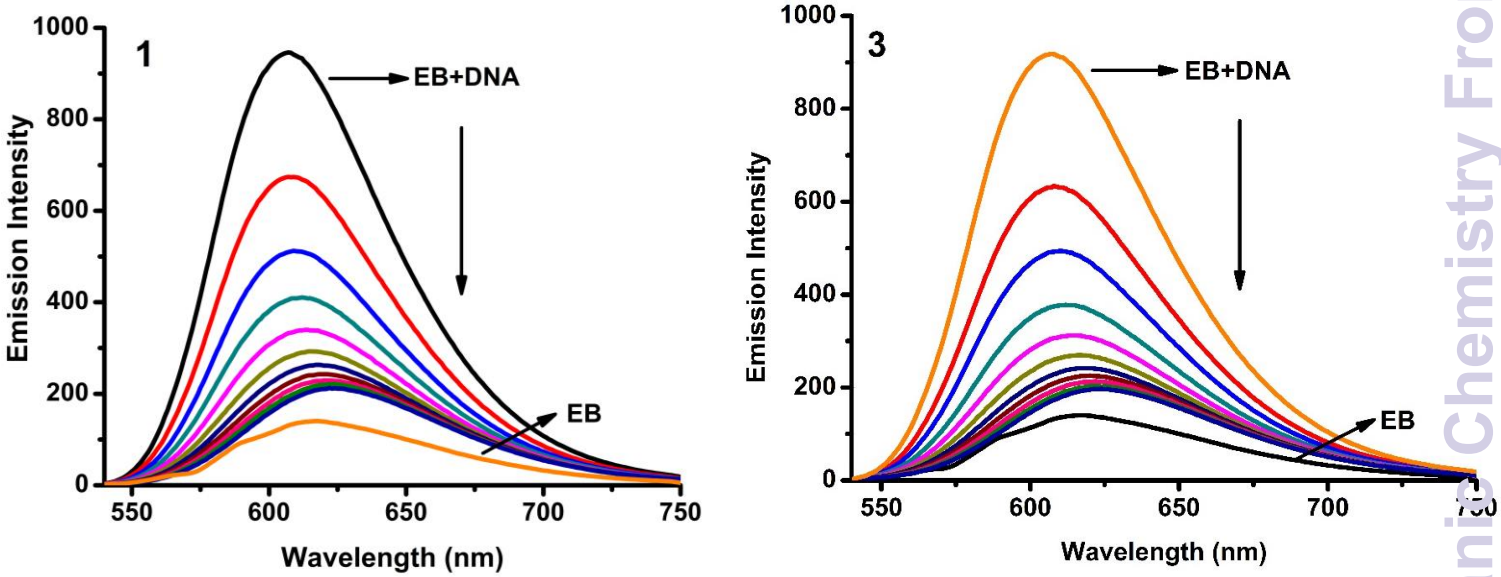

Fig. 10 Fluorescence quenching curves of EB bound to DNA in the presence of **1** and **3**. [DNA] = 5 μM, [EB] = 5 μM and [complex] = 0-50 μM.

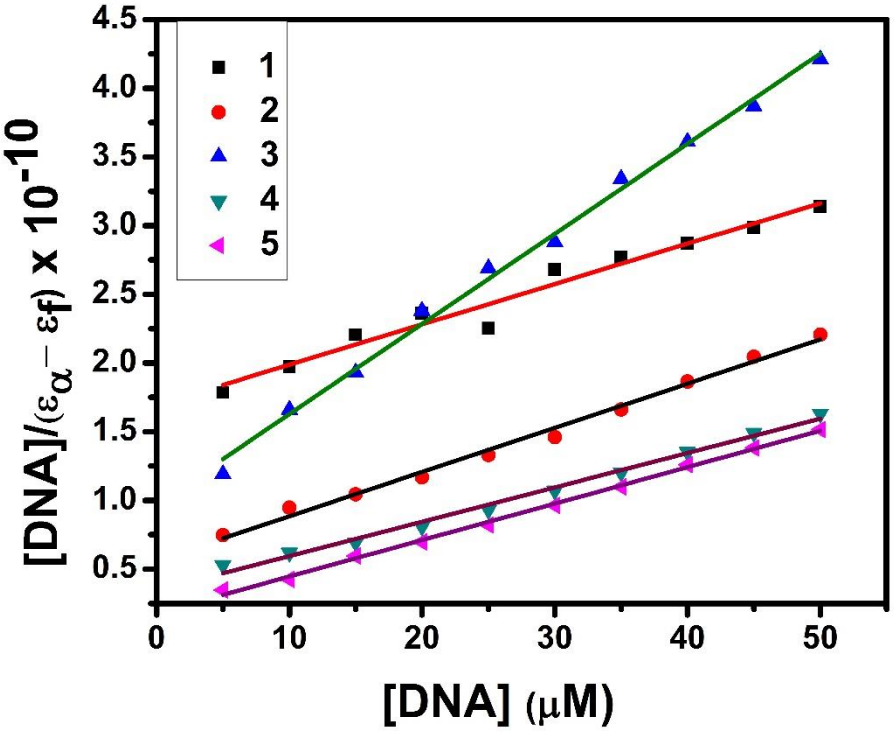

Fig. 11 Plot of [DNA]/($\varepsilon_a - \varepsilon_f$) *versus* [DNA] for the titration of the complexes with CT DNA.

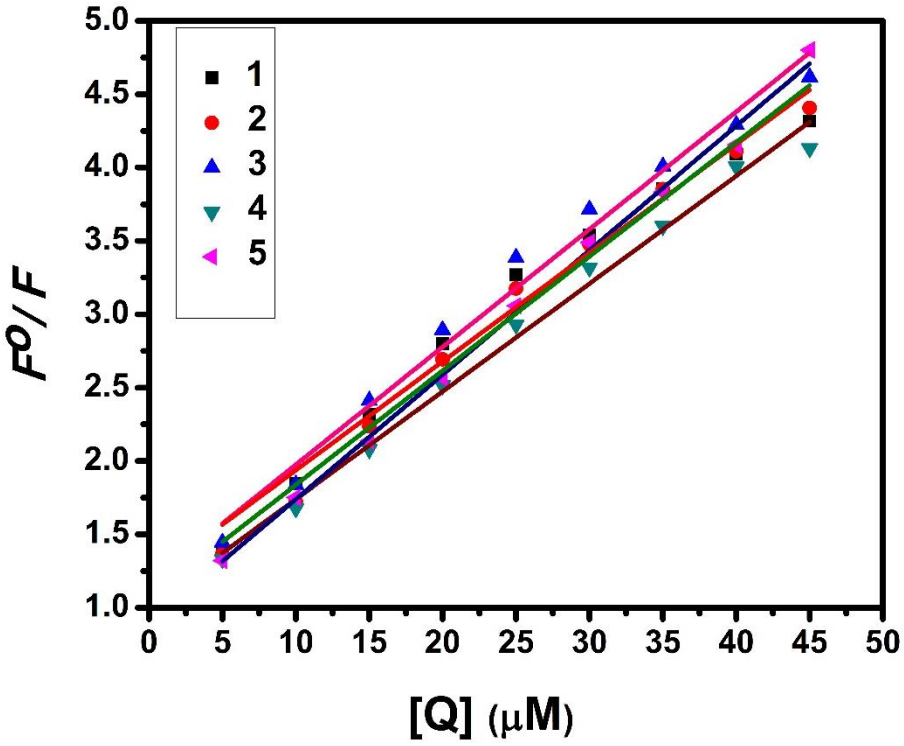

Fig. 12 Stern-Volmer plot of fluorescence titrations of the complexes with CT DNA.

(A)

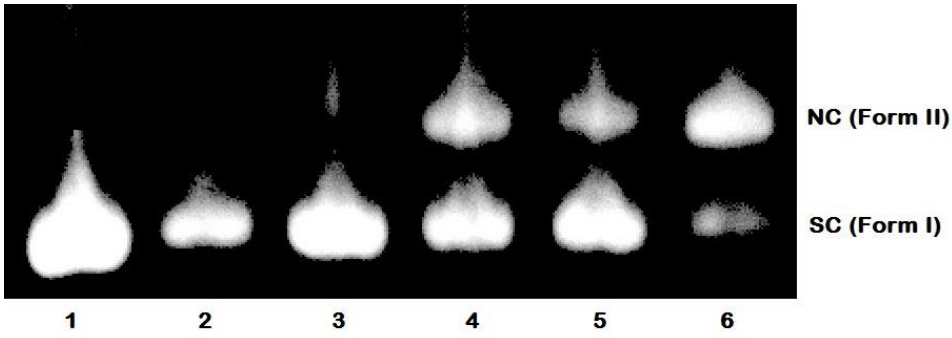

(B)

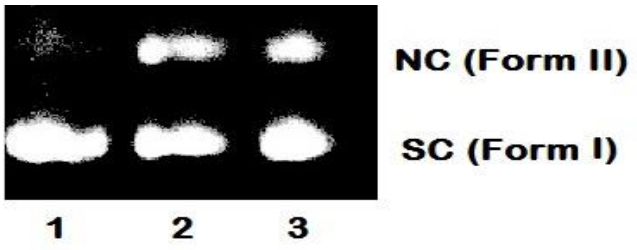

Fig. 13 Cleavage of supercoiled pBR 322 DNA (40 μM) by complexes **1**-**5** in a buffer containing 5% DMF:5 mM Tris HCl/50 mM NaCl at pH = 7.2 and 37 ℃ with an incubation time of 4 h. (A) Lane 1, DNA control; lane 2, DNA + **1** (100 μM); lane 3, DNA + **2** (100 μM); lane 4, DNA + **3** (100 μM); lane 5, DNA + **4** (100 μM); lane 6, DNA + **5** (100 μM). (B) Lane 1, DNA control; lane 2, DNA + **1** (200 μM); lane 3, DNA + **2** (200 μM). Forms SC and NC are supercoiled and nicked circular DNA, respectively.

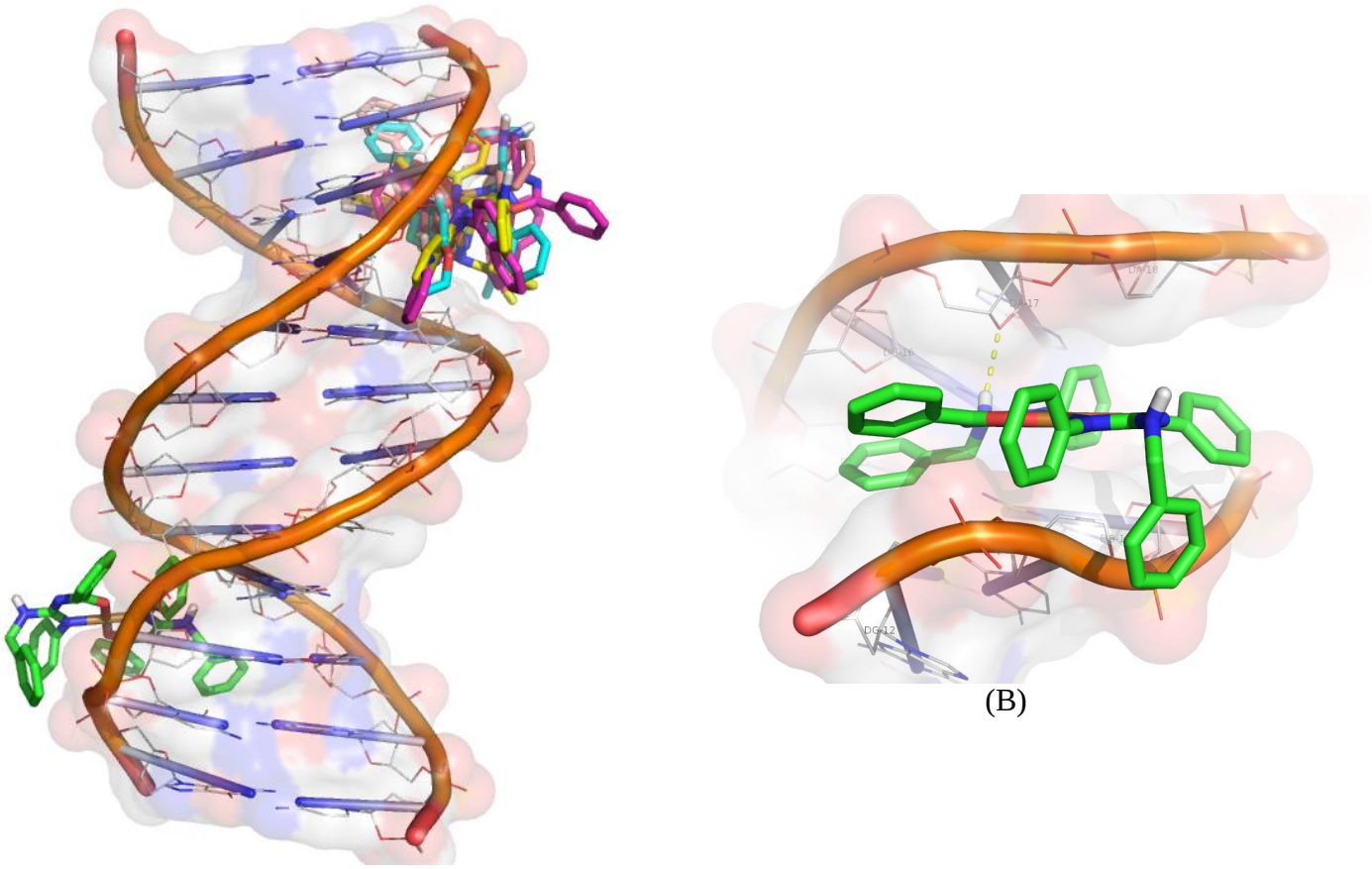

(A) (B)

Fig. 14 Molecular docked model of complexes (**1**-**5**) (A) and complex **1** (B) with DNA dodecamer duplex of sequence d(CGCGAATTCGCG)2 (PDB ID: 1BNA).

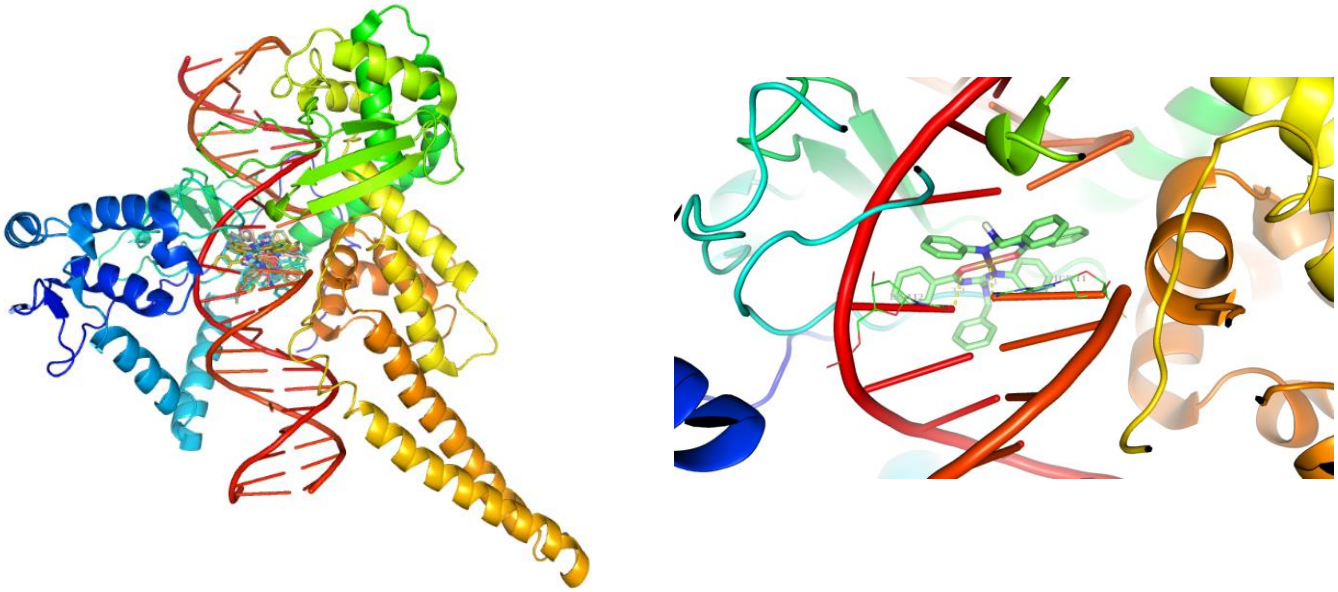

(A) (B)

Fig. 15 Molecular docked model of complexes (**1**-**5**) (A) and complex **1** (B) in the cleavage site of human DNA topoisomerase I (PDB ID:1SC7).

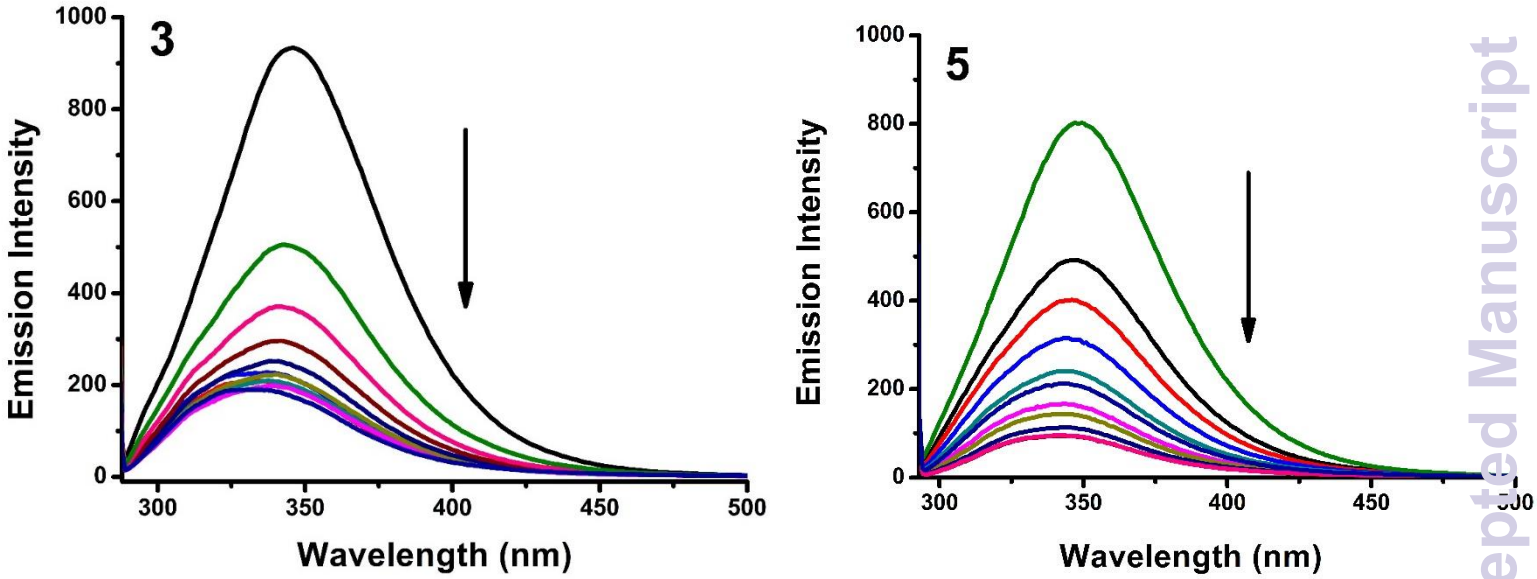

Fig.16 Fluorescence quenching curves of BSA in the absence and presence of **3** and **5**. [BSA] = 1 μM and [complex] = 0-20 μM.

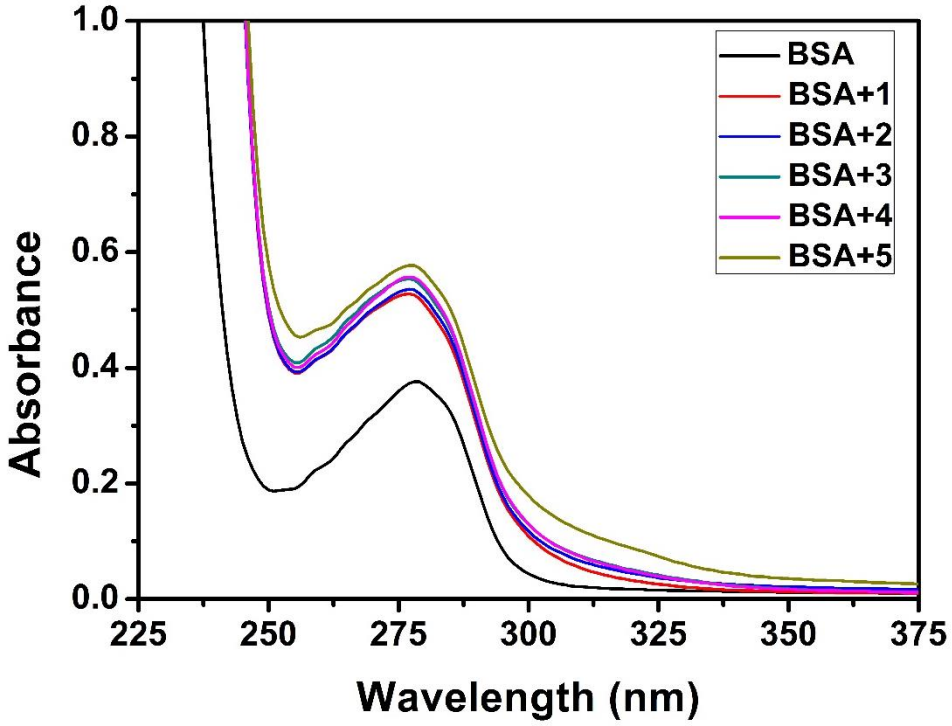

Fig. 17 The absorption spectra of BSA (10 μM) and BSA with **1**-**5** (4 μM).

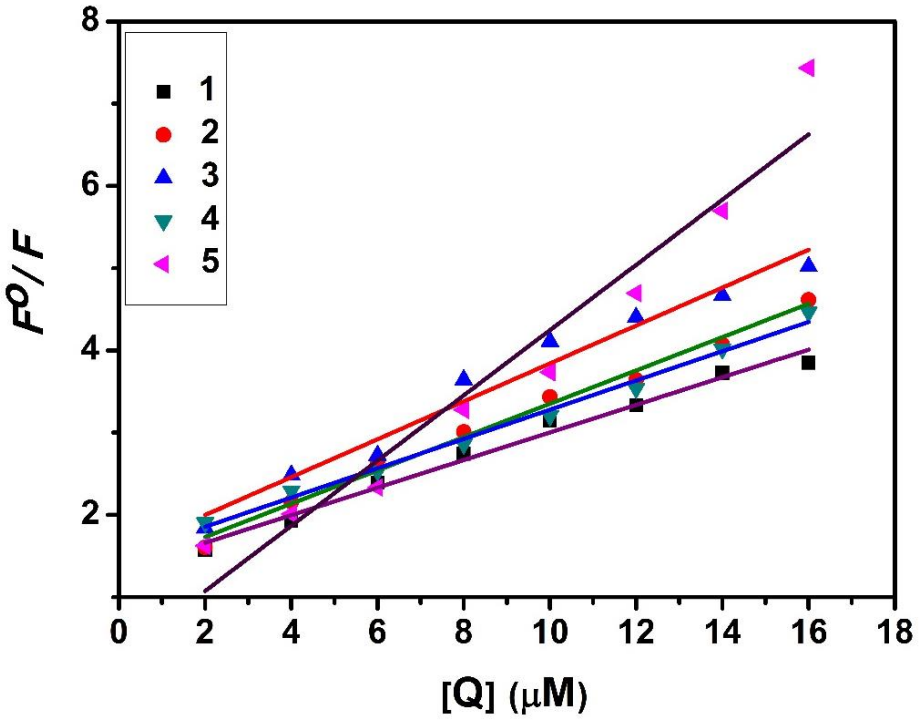

Fig. 18 Stern-Volmer plot of the fluorescence titrations of the complexes with BSA.

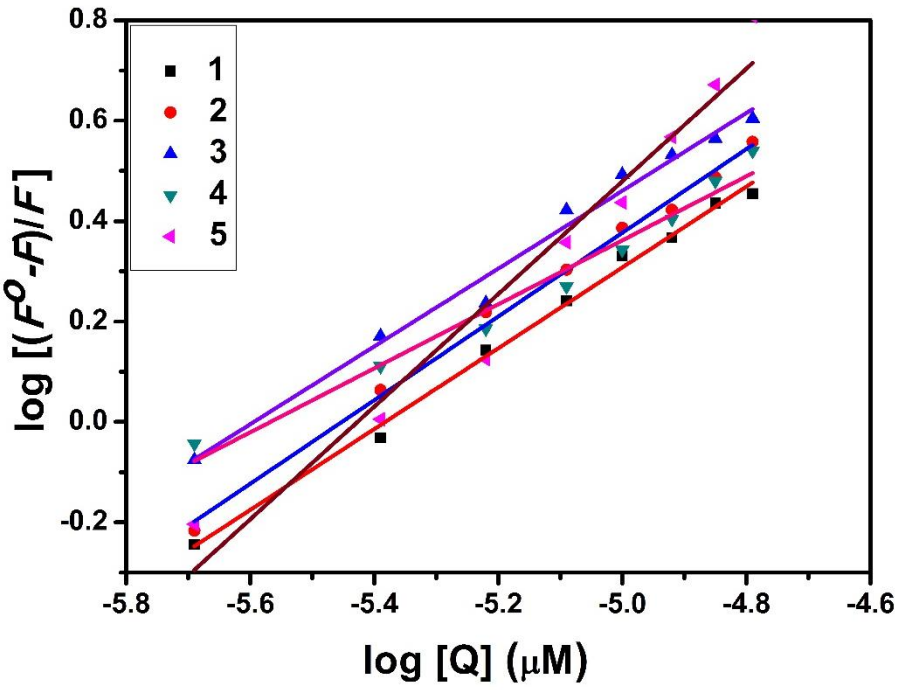

Fig. 19 Scatchard plot of the fluorescence titrations of the complexes with BSA.

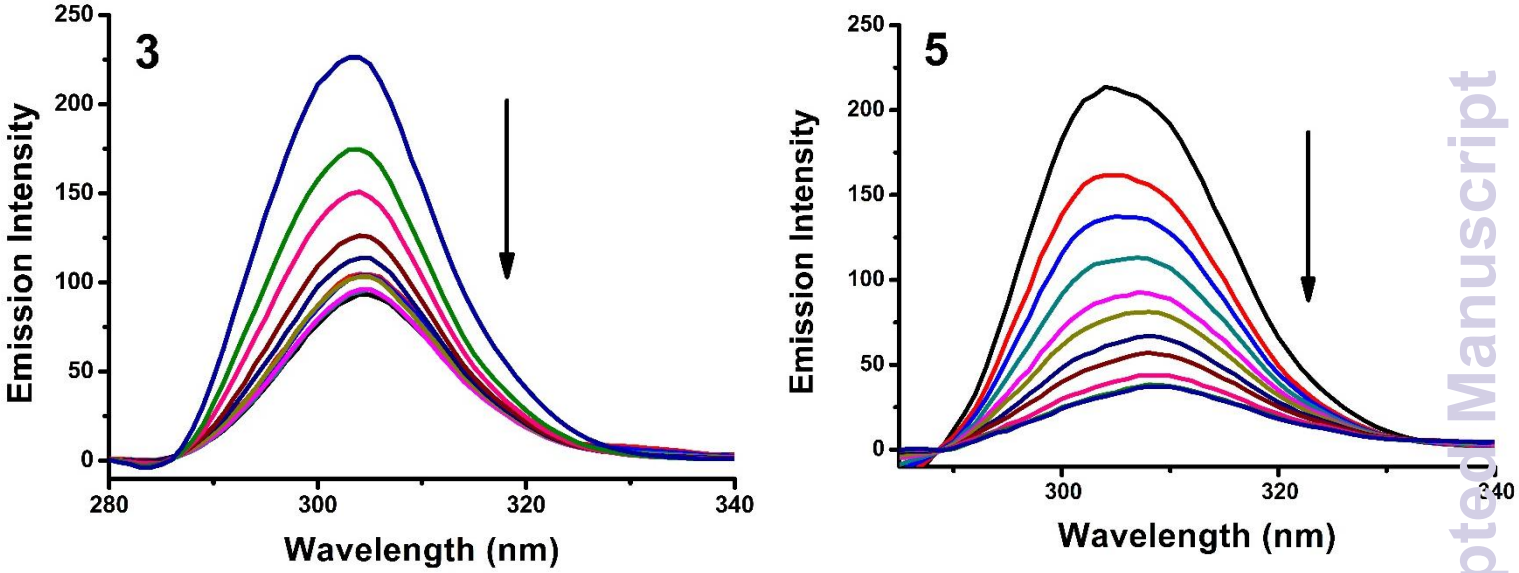

Fig. 20 Synchronous spectra of BSA (1 μM) as a function of concentration of **3** and **5** (0-20 μM) with $\Delta\lambda$ = 15 nm.

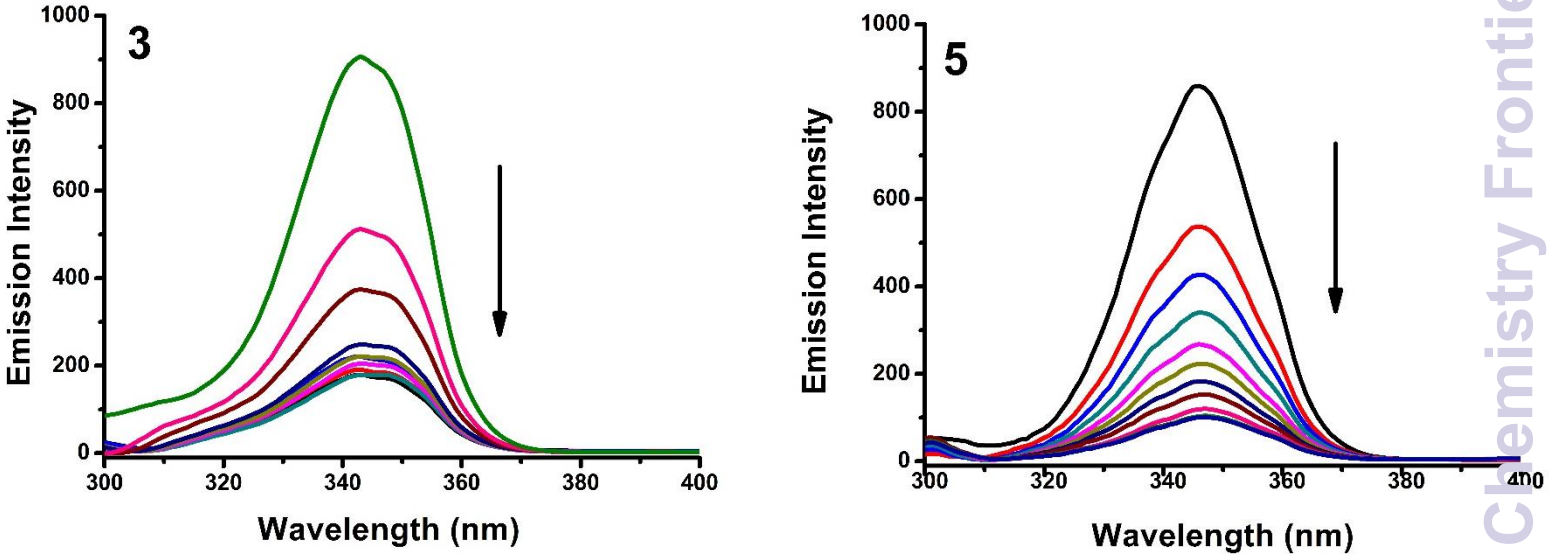

Fig. 21 Synchronous spectra of BSA (1 μM) as a function of concentration of **3** and **5** (0-20 μM) with $\Delta\lambda$ = 60 nm.

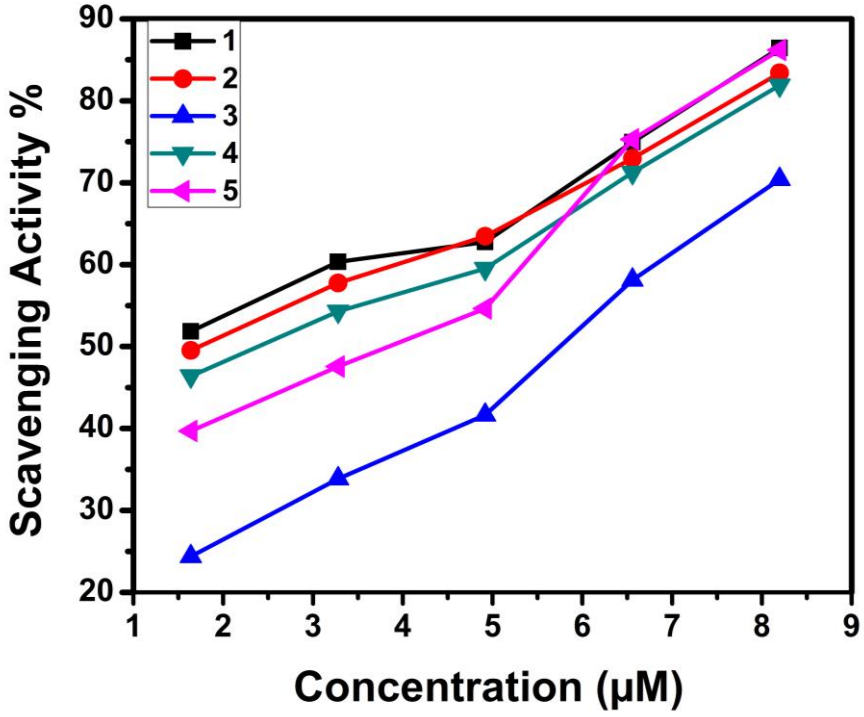

Fig. 22 Inhibition of superoxide radical by complexes **1-5**

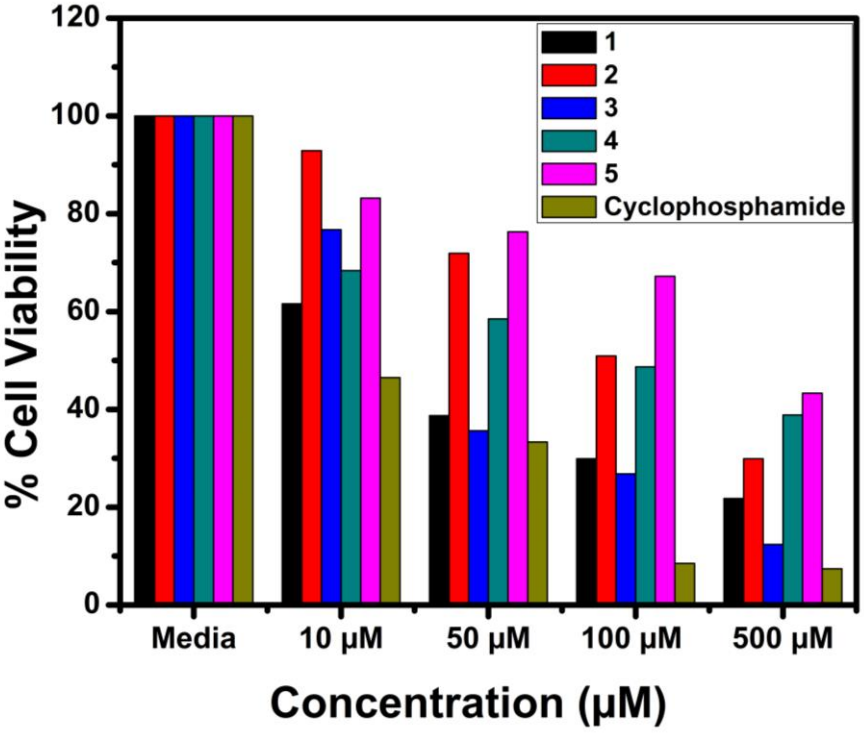

Fig. 23 Cytotoxicity of complexes **1-5** after 24 h incubation on MCF7 cell lines.

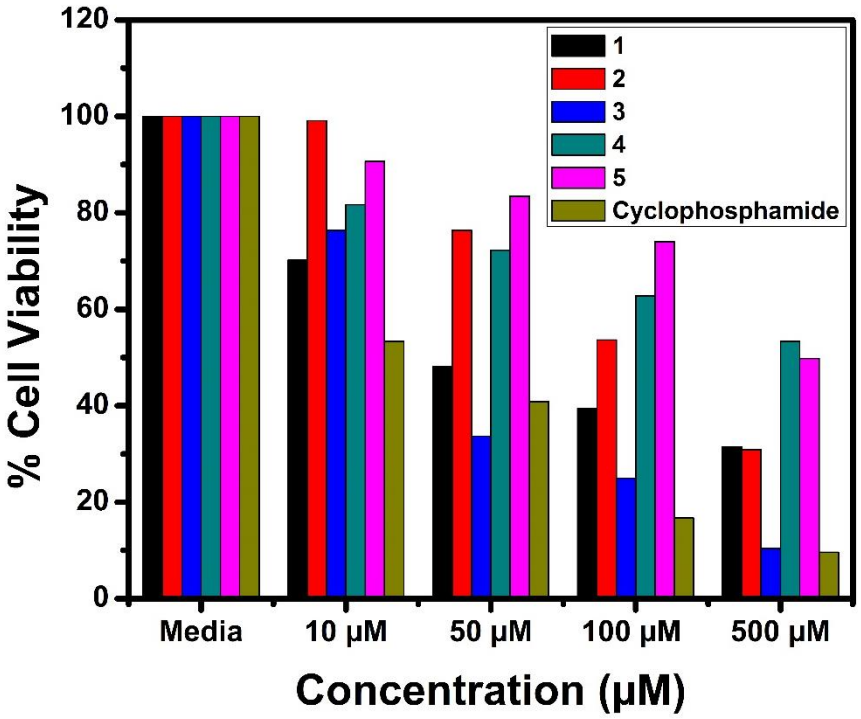

Fig. 24 Cytotoxicity of complexes **1**-**5** after 24 h incubation on A549 cell lines.

Table 1 EPR parameters of Cu(II) complexes

Complex	Medium & Temp.	$g_{\|}$	g⊥	$A_{\|}$(G)
1	Solution state LNT	2.212	2.037	174
2	Solution state LNT	2.162	2.024	178
3	Solution state LNT	2.198	2.040	180
4	Solution state LNT	2.210	2.024	161
5	Solution state LNT	2.213	2.015	172

Table 2 Crystallographic data and refinement parameters for ligands L1-L5

	L1	**L2**	**L3**	**L4**	**L5**
Empirical formula	$C_{21}H_{19}N_3O$	$C_{22}H_{21}N_3O$	$C_{23}H_{23}N_3O_2$	$C_{22}H_{21}N_3O_2$	$C_{25}H_{21}N_3O$
Formula weight	329.39	343.42	373.44	359.42	379.45
Temperature (K)	110(2)	150(2)	296.15	110(2)	110(2)
Wavelength (Å)	0.71073	0.71073	0.71073	1.54178	1.54178
Crystal system	Triclinic	Triclinic	Monoclinic	Trigonal	Triclinic
Space group	*P-1*	*P-1*	*P 1 21/c 1*	*P3(2)*	*P-1*
Unit cell dimensions					
a (Å)	8.4339(17)	12.6374(15)	10.8758(16)	9.9964(3)	10.2809(9)
b (Å)	10.588(2)	12.7890(15)	18.848(3)	9.9964(3)	10.3681(9)
c (Å)	10.687(2)	12.8040(15)	9.4682(14)	16.0766(7)	10.6801(9)
α (°)	66.082(2)	73.447(2)	90	90	62.458(5)
β (°)	82.662(2)	75.957(2)	92.429(2)	90	79.593(5)
γ (°)	82.739(2)	74.303(2)	90	120	70.395(6)
Volume ($Å^3$)	862.4(3)	1878.7(4)	1939.2(5)	1391.27(8)	950.45(14)
Z	2	4	4	3	2
Density (calculated) Mg/m^3	1.269	1.214	1.279	1.287	1.326
Absorption coefficient (mm^{-1})	0.080	0.076	0.083	0.672	0.649
F(000)	348	728	792	570	400

Crystal size (mm^3)	0.56 x 0.52 x 0.25	0.65 x 0.61 x 0.53	0.519 x 0.512 x 0.206	0.16 x 0.04 x 0.04	0.12 x 0.06 x 0.04
Theta range for data collection (°)	2.31 to 27.33	1.70 to 27.50	1.87 to 28.43	5.80 to 59.99	4.57 to 59.99
Index ranges	-10<=h<=10, -13<=k<=13, -13<=l<=13	-16<=h<=16, -16<=k<=16, -16<=l<=16	-14<=h<=14, -24<=k<=24, -12<=l<=12	-11<=h<=11, -11<=k<=11, -17<=l<=17	-11<=h<=11, -11<=k<=11, -11<=l<=11
Reflections collected	9848	25111	22873	31224	16951
Independent reflections [R(int)]	3835[R(int) = 0.0212]	8452 [R(int) = 0.0273]	4741 [R(int) = 0.0327]	2729 [R(int) = 0.0526]	2765 [R(int) = 0.0394]
Completeness to theta = 27.33 °27.50 ° 25.24 °59.99 ° 9.99 °	98.7 %	97.9 %	100.0 %	99.5 %	98 %
Absorption correction	Semi-empirical from equivalents	Semi-empirical from equivalents	Semi-empirical from equivalents	Semi-empirical from equivalents	Semi-empirical from equivalents
Max. and min. transmission	0.9803 and 0.9566	0.9608 and 0.9522	0.7457 and 0.6776	0.9736 and 0.9000	0.9745 and 0.9262
Refinement method	Full-matrix least-squares on F^2	Full-matrix least-squares on F^2	Full-matrix least-squares on F^2	Full-matrix least-squares on F^2	Full-matrix least-squares on F^2
Data / restraints / parameters	3835 / 0 / 226	8452 / 0 / 471	4741 / 0 / 254	2729 / 1 / 246	2765 / 0 / 263
Goodness-of-	1.065	1.045	1.052	1.111	1.084

fit on F^2					
Final R indices [I>2sigma(*I*)]	R1 = 0.0396, wR2 = 0.0977	R1 = 0.0424, wR2 = 0.1098	R1 = 0.0398, wR2 = 0.0972	R1 = 0.0275, wR2 = 0.0686	R1 = 0.0338, wR2 = 0.0911
R indices (all data)	R1 = 0.0464, wR2 = 0.1023	R1 = 0.0513, wR2 = 0.1153	R1 = 0.0497, wR2 = 0.1036	R1 = 0.0285, wR2 = 0.0692	R1 = 0.0390, wR2 = 0.0939
Largest diff. peak and hole ($e.Å^{-3}$)	0.261 and -0.228	0.282 and -0.267	0.254 and -0.221	0.125 and -0.127	0.158 and -0.222

Table 3 Crystallographic data and refinement parameters for complexes (**1** and **2**)

	1	**2**
Empirical formula	$C_{42}H_{36}CuN_6O_2$	$C_{44}H_{40}CuN_6O_2$
Formula weight	720.31	748.36
Temperature (K)	150(2)	150(2)
Wavelength (Å)	0.71073	0.71073
Crystal system	Triclinic	
Space group	*P-1*	*P-1*
Unit cell dimensions		
a (Å)	8.4363(13)	6.1250(8)
b (Å)	10.3390(16)	11.5140(14)
c (Å)	10.9129(17)	13.2365(16)
α (°)	65.535(2)	81.520(2)
β (°)	86.346(2)	87.731(2)
γ (°)	85.211(2)	85.984(2)
Volume ($Å^3$)	862.9(2)	920.6(2)
Z	1	1
Density (calculated) Mg/m^3	1.386	1.350
Absorption coefficient (mm^{-1})	0.680	0.640

F(000)	375	391
Crystal size (mm^3)	0.18 × 0.14 × 0.04	0.45 × 0.21 × 0.21
Theta range for data collection	2.05 to 27.50	1.56 to 27.49
Index ranges	-10<=h<=10, -13<=k<=13, -14<=l<=14	-7<=h<=7, -14<=k<=14, -17<=l<=17
Reflections collected	14794	19956
Independent reflections	3925 [R(int) = 0.0485]	4161 [R(int) = 0.0214]
Completeness to theta = 27.50 °	99.1 %	98.7 %
Absorption correction	Semi-empirical from equivalents	Semi-empirical from equivalents
Max. and min. transmission	0.9733 and 0.8874	0.8773 and 0.7616
Refinement method	Full-matrix least-squares on F^2	Full-matrix least-squares on F^2
Data / restraints / parameters	3925 / 0 / 232	4161 / 0 / 242
Goodness-of-fit on F^2	1.079	1.071
Final R indices [I>2sigma(*I*)]	R1 = 0.0317, wR2 = 0.0846	R1 = 0.0258, wR2 = 0.0677
R indices (all data)	R1 = 0.0326, wR2 = 0.0853	R1 = 0.0266, wR2 = 0.0684
Largest diff. peak and hole ($e.Å^{-3}$)	0.441 and -0.427	0.294 and -0.272

Table 4 Selected bond lengths (Å), angles (°) of ligands

	L1	**L2**	**L3**	**L4**	**L5**
O(1)-C(2)	1.2453(13)	1.2521(14)	1.2442(14)	1.2562(19)	1.2513(16)
N(1)-C(1)	1.3281(14)	1.3407(14)	1.3313(14)	1.3387(19)	1.3352(17)
N(1)-C(2)	1.3591(14)	1.3438(15)	1.3526(14)	1.3470(17)	1.3570(17)
N(2)-C(1)	1.3509(14)	1.3484(15)	1.3464(14)	1.3360(2)	1.3470(17)
N(2)-C(9)	1.4483(14)	1.4186(14)	1.4331(14)	1.4550(2)	1.4239(17)
N(3)-C(1)	1.3460(14)	1.3358(15)	1.3449(14)	1.3460(2)	1.3451(17)
N(3)-C(16)	1.4281(14)	1.4520(16)	1.4920(13)	1.4320(2)	1.4527(17)
N(2)-H(2)	0.8899	0.8800	0.8800	0.8800	0.8800
N(3)-H(3)	0.8934	0.8800	0.8800	0.8800	0.8800

C(1)-N(1)-C(2)	120.15(9)	120.55(10)	120.46(9)	120.23(13)	120.51(11)
C(1)-N(2)-C(9)	123.78(9)	129.58(10)	123.00(9)	122.78(12)	128.41(11)
C(1)-N(2)-H(2)	114.9	115.20	118.50	117.90	115.80
C(9)-N(2)-H(2)	114.9	115.20	118.50	117.90	115.80
C(1)-N(3)-C(16)	123.71(9)	122.20(10)	122.95(9)	124.19(13)	123.16(11)
C(1)-N(3)-H(3)	121.2	118.90	118.50	118.60	118.40
C(16)-N(3)-H(3)	121.2	118.90	118.50	118.60	118.40
N(1)-C(1)-N(3)	125.53(10)	122.95(10)	126.17(10)	124.43(14)	123.48(12)
N(1)-C(1)-N(2)	117.36(10)	117.33(10)	116.78(10)	117.82(13)	117.44(12)
N(3)-C(1)-N(2)	117.08(10)	119.70(10)	117.01(10)	117.74(13)	119.08(12)
O(1)-C(2)-N(1)	126.88(10)	126.77(10)	127.35(10)	127.06(14)	127.03(12)
O(1)-C(2)-C(3)	119.33(10)	118.83(10)	119.17(9)	118.02(14)	118.99(11)
N(1)-C(2)-C(3)	113.79(9)	114.40(10)	113.47(9)	114.92(13)	113.98(11)
N(2)-C(9)-C(10)	114.44(9)	115.95(10)	114.39(9)	113.88(13)	114.63(11)
N(2)-C(9)-H(9A)	108.6	108.30	108.70	108.80	108.60(11)
N(2)-C(9)-H(9B)	108.6	108.30	108.70	108.80	108.60(11)

Table 5 Selected bond lengths (Å), angles (°) of complexes

	1	**2**
Cu(1)-O(1)	1.9055(11)	1.9122(9)
Cu(1)-O(1)#1	1.9055(11)	1.9122(9)
Cu(1)-N(1)	1.9752(13)	1.9602(10)
Cu(1)-N(1)#1	1.9752(13)	1.9602(10)
O(1)-Cu(1)-N(1)	89.69(5)	90.03(4)
O(1)#1-Cu(1)-N(1)#1	89.65(5)	90.04(4)
O(1)#1-Cu(1)-N(1)	90.31(5)	89.97(4)
O(1)-Cu(1)-N(1)#1	90.31(5)	89.96(4)
O(1)#1-Cu(1)-O(1)	180.0	180.0
N(1)-Cu(1)-N(1)#1	180.0	180.0
C(2)-O(1)-Cu(1)	128.05(10)	125.59(8)

C(1)-N(1)-Cu(1)	124.39(9)	123.25(8)
C(3)-N(1)-Cu(1)	119.49(9)	120.29(7)

Symmetry transformations used to generate equivalent atoms: #1 -x,-y,-z

Table 6 DNA binding constant (K_b), quenching constant (K_q) and apparent binding constant (K_{app}) values

Complex	K_b (M^{-1})	K_q (M^{-1})	K_{app} (M^{-1})
1	7.69×10^4	8.28×10^4	4.14×10^6
2	6.63×10^4	8.11×10^4	4.05×10^6
3	1.63×10^5	8.37×10^4	4.18×10^6
4	5.62×10^4	7.86×10^4	3.93×10^6
5	1.67×10^4	7.73×10^4	3.86×10^6

Table 7 Molecular docking parameters of complexes **1-5** with B-DNA (PDB ID: 1BNA) dodecamer $d(CGCGAATTCGCG)_2$

Complex	**Final intermolecular energy kcal/mol**			**Final total internal energy (2) kcal/mol**	**Torsional free energy (3) kcal/mol**	**Unbound system's energy [=(2)] (4) kcal/mol**	**Estimated free energy of binding [(1)+(2)+(3)-(4)] kcal/mol**
	vdW + Hbond + desolv energy	**Electrostatic energy**	**Total (1)**				
1	-10.24	-1.38	-11.62	-4.24	+2.74	-4.24	-8.88
2	-9.23	-0.02	-9.25	-6.33	+2.47	-6.33	-6.78
3	-9.55	-0.00	-9.56	-6.74	+3.84	-6.74	-5.71
4	-8.90	-0.16	-9.05	-6.13	+2.74	-6.13	-6.31
5	-9.99	-0.02	-9.96	-7.67	+2.74	-7.67	-7.22

Table 8 Molecular docking parameters of complexes (**1-5**) with human-DNA-Topo-I complex (PDB ID: 1SC7)

Complex	Final intermolecular energy kcal/mol			Final total internal energy (2) kcal/mol	Torsional free energy (3) kcal/mol	Unbound system's energy [=(2)] (4) kcal/mol	Estimated free energy of binding [(1)+(2)+(3)-(4)] kcal/mol
	vdW + Hbond + desolv energy	Electrostatic energy	Total (1)				
1	-13.41	-0.10	-13.51	-3.83	+2.74	-3.83	-10.77
2	-12.93	+0.04	-12.89	-5.81	+2.47	-5.81	-10.42
3	-14.50	-0.03	-14.53	-5.79	+3.84	-5.79	-10.69
4	-13.49	+0.01	-13.48	-5.85	+2.74	-5.85	-10.74
5	-14.76	-0.04	-14.80	-5.41	+2.74	-5.41	-12.05

Table 9 Protein binding constant (K_b), quenching constant (K_q) and number of binding sites (n) values

Complex	K_b (M^{-1})	K_q (M^{-1})	n
1	7.09×10^{3}	1.52×10^{5}	0.6942
2	5.42×10^{4}	2.25×10^{5}	0.8693
3	2.15×10^{4}	2.30×10^{5}	0.7747
4	1.60×10^{4}	1.94×10^{5}	0.7809
5	2.49×10^{6}	4.33×10^{5}	1.1799

Table 10 IC_{50} values (μM) calculated from SOD assays of Cu(II) complexes (**1-5**)

Complex	IC_{50} (μM)
1	1.53
2	1.78
3	5.62
4	2.66
5	3.58

Table 11 *In vitro* cytotoxicity of the Cu(II) complexes in MCF7, A549 and NIH 3T3 cell lines

Compound	IC_{50} (μM)		
	MCF7	**A549**	**NIH 3T3**
1	42.71	52.98	900.34
2	107.02	122.2	723.40
3	37.1	45.71	600.30
4	204.52	256.32	572.81
5	198.6	232.6	670.22
Cyclophosphamide	11.89	41.81	-